HALOGENATED TAGS FOR THE INVESTIGATION OF ENZYME SPECIFICITY

by

Hailey Houde

A thesis submitted to the faculty of
The University of North Carolina at Charlotte
in partial fulfillment of the requirements
for the degree of Master of Science in
Chemistry

Charlotte

2023

Approved by:

_____
Dr. Jerry Troutman

_____
Dr. Thomas Schmedake

_____
Dr. Donald Jacobs

_____
Dr. Joanna Krueger

©2023
Hailey Houde
ALL RIGHTS RESERVED

ABSTRACT

HAILEY HOUDE. Halogenated Tags for The Investigation of Enzyme Specificity.
(Under the direction of DR. JERRY TROUTMAN)

The bacterial enzyme undecaprenyl pyrophosphate synthase (UppS) is present in most prokaryotes and is needed for bacterial survival. UppS produces the essential lipid carrier, bactoprenyl monophosphate (BP). BP is critical for the structural integrity of cell membranes, the supply and storage of energy, and antibacterial resistance. Therefore, a greater understanding of this enzymes active site would provide insight into an important target for new therapeutics directed at pathogenic microorganisms. This study investigated the specificity and selectivity of UppS through the modification of its natural substrate, farnesyl diphosphate (FPP). Previous studies utilized mutations of specific residues within the active site, however, mutating protein sequences can have deleterious effects on structure that can often be difficult to recognize. Altering a natural UppS substrate allows a more controlled investigation of the active site. Herein, a group of carefully selected halogenated aromatics were chosen to synthesize in order to test the selectivity of the enzyme based on size, electronegativity, and shape. The effect of the tags' shape on enzyme activity was investigated through the appendage of the halogen in the para position of an aniline ring appended to the end of the molecule. The effect of size and electronegativity on enzyme activity was also investigated using halogenated-aniline rings coupled to the molecular probes. The analogues used were formed via a five-step synthesis process that includes reductive amination and diphosphorylation reactions. The halogenated FPP analogue 4BrGPP was tested with UppS from the organism *Staphylococcus aureus*.

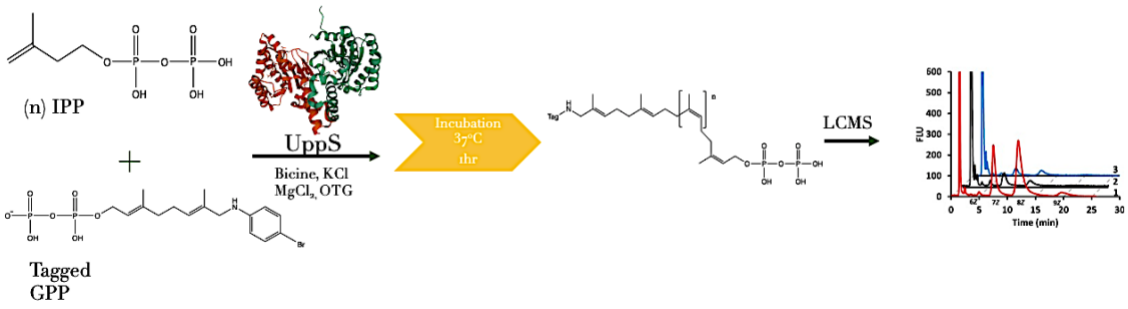
(n) IPP
Tagged GPP
UppS
Bicine, KCl
MgCl2, OTG
Incubation
37°C
1hr
LCMS
FLU
Time (min)
3
2
1

ACKNOWLEDGMENTS

I would like to thank the current and past members of the Troutman Lab for their guidance. First, I would like to thank Dr. Amanda Reid for sharing her expertise in organic synthesis, HPLC, and NMR analysis. You helped me grow my critical thinking and problem solving skills, which have been critical to my success as a graduate student. To Beth Scarbrough, for training me on the LCMS and for always answering my questions no matter how seemingly small they were. I would also like to thank Theresa Black for always being so immensely supportive throughout this rollercoaster of higher education. To Alexis Murray, for her patience and great listening skills when an experiment didn't go quite right for me. I couldn't be more thankful for this experience and all the wonderful friendships made along the way.

Finally, thank you to my committee members who have been supportive throughout my entire journey. Thank you, Dr. Vivero-Escoto for asking eye-opening questions about my research that led me down a new path. Thank you, Dr. Jacobs for your help and support with computational and structural biology. You introduced me to Pymol which was extremely helpful when investigating the active site of UppS. Thank you Dr. Indrasekara, for your sharing your immense knowledge on instrumental analysis and for your guidance in my first year as a graduate student. Thank you, Dr. Krueger for your willingness to join my committee in my third semester! Thank you to Dr. Schmedake for saving the day by joining my committee at the last minute. And lastly, I cannot thank Dr. Troutman enough for being such a wonderful research mentor. You introduced me to the world of biochemistry and I am so grateful for that. Because of your support and passion for biochemistry, I know that I want a research-focused career.

DEDICATION

For my family and Josh, I could have never done this without all of your unconditional love and support.

TABLE OF CONTENTS

LIST OF TABLES

LIST OF FIGURES

LIST OF ABBREVIATIONS

Ala	Alanine
Arg	Arginine
Asn	Asparagine
Asp	Aspartic Acid
BP	Bactoprenyl phosphate
BPP	Bactoprenyl diphosphate
ddd	doublet of doublets of doublets
E. coli	*Escherichia coli*
EN	Electronegativity
FC	Flash chromatography
FsPP	(S)-Farnesyl thiopyrophosphate
FPP	Farnesyl diphosphate
FTase	Farnesyl transferase
Gly	Glycine
GOAc	Geranyl acetate

GOH	Geranyl alcohol
GPP	Geranyl diphosphate
GCMS	Gas Chromatography Mass Spectrometry
His	Histidine
HPLC	High Performance Liquid Chromatography
Ile	Isoleucine
IPP	Isopentenyl diphosphate
IPTG	Isopropyl β- d-1-thiogalactopyranoside
LCMS	Liquid Chromatography Mass Spectrometry
Leu	Leucine
MRSA	Methicillin-resistant *staphylococcus aureus*
MSQ	Mass Spectrometry Quadrupole
NaCl	Sodium Chloride
OTG	Octylthioglucoside
TLC	Thin layer chromatography

td	Triplet of doublets
UppP	Undecaprenyl Pyrophosphate Phosphatase
UppS	Undecaprenyl Pyrophosphate Synthase
$UppS_{Bf}$	Undecaprenyl Pyrophosphate Synthase from *Bacteroides fragilis*
$UppS_{Ec}$	Undecaprenyl Pyrophosphate Synthase from *Escherichia coli*
$UppS_{Sa}$	Undecaprenyl Pyrophosphate Synthase from *Staphylococcus aureus*
$UppS_{Vv}$	Undecaprenyl Pyrophosphate Synthase from *Vibrio vulnificus*
Val	Valine

CHAPTER 1: INTRODUCTION

1.1: Bacterial Glycans in Bacteriology

Glycans are complex sugar polymers and oligomers that are produced by both Gram-negative and Gram-positive bacterial species that are crucial for the supply and storage of energy as well as the structural integrity of the cell wall. The biological roles of these polymers are extraordinarily diverse, including host invasion and colonization, virulence activity, and contributions to antibacterial resistance.[1,2] Of these polymers, peptidoglycan is most notable. It is a complex polymer of sugars and peptides essential for bacterial cell wall construction and therefore is a key target for major antibiotics including penicillin. While these polymers are of interest in bacteriology, they can be difficult to work with, causing investigations of their biological roles and uses in biotechnology to be far behind those of other major biological polymers, such as nucleic acids and proteins.

Bacterial glycan structures are extremely diverse and are essential to most life forms and are responsible for key biological roles.[1] Unlike proteins and nucleic acids, the synthesis of these polymers and oligosaccharides is not template dependent, which is a major reason that our understanding of their function lags so far behind the other major biological polymers. While the biosynthesis of bacterial glycans is not template mediated, there are common components between polysaccharide biosynthesis pathways. The one thing most bacterial glycans have in common is that they are synthesized on a 55-carbon isoprenoid scaffold called bactoprenyl monophosphate (BP).[2] Bactoprenyl monophosphate serves as an essential lipid carrier and is critical in early polysaccharide bioassembly (**Figure 1**).[3,4] BP localizes early steps of polysaccharide synthesis to the cytoplasmic leaflet

of the bacterial inner membrane where a series of pathway dependent enzymes assemble the glycans one sugar at a time.

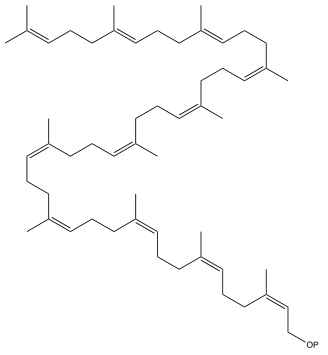

Figure 1*:* Bactoprenyl monophosphate structure

BP is produced in bacteria by the enzyme undecaprenyl pyrophosphate synthase (UppS) and undecaprenyl pyrophosphate phosphatase (UppP) (**Figure 2**).[4] UppS catalyzes an ordered series of reactions in which first the 15-carbon isoprenoid farnesyl diphosphate (FPP) binds to the active site of the enzyme followed by sequential additions of eight five-carbon isoprenoid units from the donor isopentenyl diphosphate. Because UppS is critical to the assembly of these important glycans, the development of inhibitors of this enzyme could be crucial to the development of new antimicrobial agents. A greater understanding of the UppS active site and the chemical interactions of its substrates would provide insight into this important target for new therapeutics directed at pathogenic microorganisms.

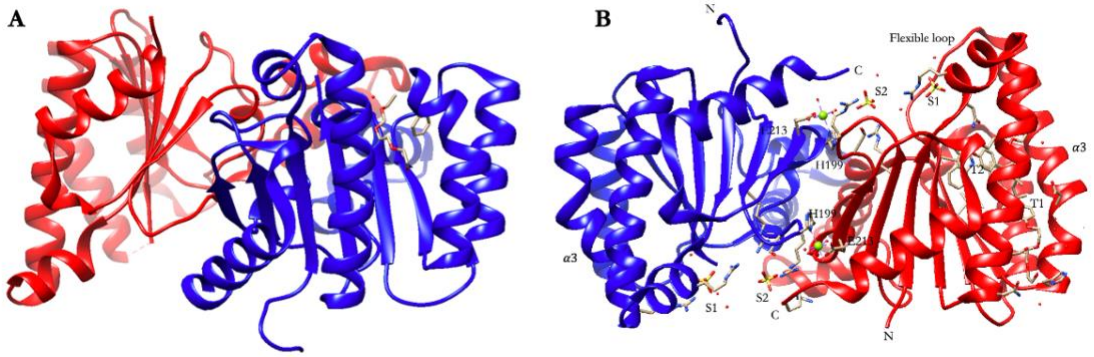

Figure 2*: A) Structure of UppS obtained from Escherichia coli.(PDB 1JP3). B) UppS active site with 2 bound sulfate ions, S1 and S2, and two bound triton molecules T1 and T2. (PDB 1UEH)*

Often, the investigation of the active site of proteins employs site directed mutagenesis to alter specific amino acids associated with protein function.[5,6] However, altering amino acid structures with natural amino acids can be limiting, and close examination of structure/activity relationships can be met with difficulty due to the limited chemical space that can be explored. Additionally, altering amino acid structures can alter protein folding patterns that are difficult to detect. In turn, residues that may appear to be required for function instead just induce misfolding.[7,8] Misfolding of proteins is responsible for several prion diseases where the infectious agent is the misfolding itself. Some of these prion diseases include Alzheimer's disease, Pick's disease, and Mad Cow disease.[9,10] To avoid protein misfolding, an alternative to site-directed- mutagenesis can be used. This alternative method for investigating enzyme active sites is to use careful structure alteration of the enzyme substrate. Such alterations are not limited to just a set of 20 amino acids and could include various types of functionality to probe the enzyme active site.[11] This thesis aims to investigate the specificity and selectivity of the UppS enzyme through the

modification of the natural substrate farnesyl diphosphate (FPP) with carefully selected halogenated aromatics that test the selectivity of the enzyme based on size, electronegativity, and shape.

1.2: UppS Structure and Function

Bacterial resistance to current antibiotics has been the impetus for research into enzymes responsible for bacterial peptidoglycan synthesis.[12] UppS, with its conserved overall structure, is present in nearly all bacterial species. UppS is a cis-prenyltransferase that generates primarily C_{55} long chains (bactoprenyl diphosphate). The terminal phosphate is then cleaved to afford bactoprenyl monophosphate (BP), the essential lipid carrier. Understanding the structure of UppS has been an area of interest for researchers, especially for the purposes of new antibiotic design.

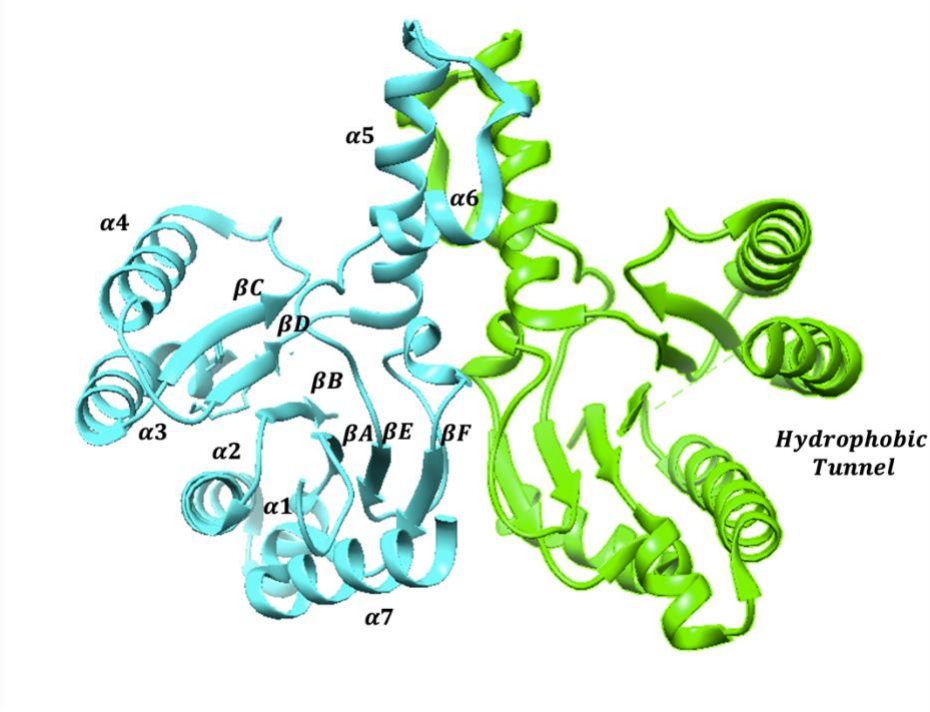

***Figure 3**: UppS ribbon structure. Monomer A in cyan blue, and monomer B in lime green.*

UppS is a homodimer where each monomer contains two α-helices (α2 and α3) and four β-sheets (βA,βB,βC,βD) that form a hydrophobic tunnel (**Figure 3**).[13,14] There is a flexible loop consisting of 12 amino acid residues above the α3 helix that pulls the helix closer to the α2 helix encapsulating the hydrophobic tunnel.[15,16]The movement of these two helices closer together causes the enzyme to enter its "closed" conformation where the substrates and enzyme more readily interact for catalysis.[15,16,17]

In 2003 Chang et al. reported on UppS complexed with sulfate ions, magnesium ions, and Triton X-100 to investigate how the metal ion affected catalysis and what function the flexible loop performed in the process.[13] The crystal structure shows that during substrate binding and release, UppS undergoes a conformational change.[13] Two sulfate ions were present in the active site of both "open" and "closed" monomers. The "open" monomer was distinguished by the absence of a Triton molecule in the active site. [13] The "closed" monomer was distinguished by the presence of two product-like Triton molecules.[13] One of the sulfate ions was found to have hydrogen bonds with the backbone nitrogen atoms of Gly-27, Gly-29, and Arg-30.[13] Similarly, the second sulfate ion was found to also have hydrogen bonds with the nitrogen backbone atoms of Arg-194, Arg-200. [13] The natural substrates of UppS, FPP and IPP, both share a high negatively charged moiety. Therefore, the sulfate binding site is likely the binding site of the natural farnesyl diphosphate substrate; and the location of the bound triton suggested that this was the elongation site for the bactoprenyl diphosphate product.[13]

The surfactant molecules were found in the top and bottom of the hydrophobic tunnel in monomer B. [13] The interactions between the active site residues and the surfactant molecules were mainly hydrophobic. The Triton molecule near the bottom of the tunnel

interacted with amino acid residues containing hydrophobic side chains.[13] These residues included "Ala-47, Val-50, Val-54, Ala-92, Leu-100, Leu-107, Leu-139, and Ile-14."[13] Leu-137 and Val-105 seal the bottom of the tunnel and are responsible for chain elongation determination (**Figure 4**). [13] Through kinetic studies, Chang et al. determined that at higher concentrations of Triton, the enzyme activity decreases. This was attributed to the Triton molecule binding to the active site changing the conformation from "closed" to "open", thus inhibiting enzyme activity.[13]

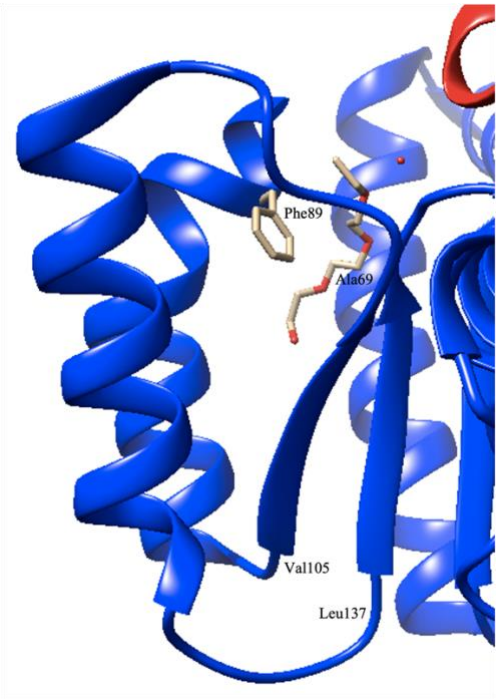

Figure 4*: Hydrophobic tunnel of UppS showing the "floor" of the tunnel sealed by Leu-137 and Val-105.*

Chang et al. also found that there were two magnesium ions were bound to equivalent positions at the dimer interface.[13] The binding of the magnesium ions led to structural changes, which in turn allowed side chain rotation of key amino acids into a more

ideal orientation for the binding of the second sulfate ion.[13] The catalytic cycle for substrate binding and product release was suggested to occur as follows: The initial binding of the farnesyl diphosphate and isopentenyl diphosphate marks the beginning of the condensation reaction.[13] The release of the diphosphate from the farnesyl diphosphate begins the condensation by adding five carbon atoms and the elongating hydrocarbon. Another isopentenyl molecule is added through a similar reaction. This continues until the C_{55} product has been reached.[13]

Two years later, Liang et. al. solved the crystal structure for UppS from *Escherichia coli* in complex with farnesyl diphosphate.[18] As the group had previously suggested, the negative moiety of the FPP diphosphate group was bound to the amine backbone of Arg-29, Gly-29, and hydrogen bonded to the side chains of Asn-28, Arg-30, and Arg-39 residues in the active site.[16] The previous studies binding region of the sulfate ion was confirmed to be the binding sites for FPP and IPP.[16] The hydrocarbon tail on the FPP substrate was found to interact with the hydrophobic side chains of residues Leu-85, Leu-88, and Phe-89.[18] To investigate the roles of these residues, Leu-85, Leu-88, and Phe-89 were mutated. [18] Replacing these three amino acids with a smaller alanine resulted in weaker hydrophobic interactions. [18] The weakened hydrophobic interactions led to an increase in K_m values for IPP and overall poor enzyme activity. [18] The decrease in enzyme activity showed that these residues are necessary for the proper positioning and orientation of the FPP substrate for nucleophilic attack by the homoallylic substrate. [18]

1.2.1: UppS Kinetics

While structure studies provide important insights into UppS function, kinetic assays provide critical information on enzyme catalysis and the dynamic interactions of substrates and products with the enzyme. To examine UppS kinetics, product distribution, and to predict the reaction mechanism, Liang and coworkers conducted UppS reactions with various concentrations of enzyme, substrates, and surfactants used to mimic a bacterial membrane.[19] In the presence of Triton-X-100 with sub-stoichiometric enzyme relative to FPP and ten equivalents of IPP the product formed by the enzyme was the natural length C_{55} bactoprenyl diphosphate (BPP). They observed a similar product with excess enzyme. However, under conditions where FPP was equivalent to IPP or in excess of IPP, smaller products were formed in the presence of surfactant. Interestingly, when the surfactant was left out of the reaction, larger products were observed. Using transient-state kinetics experiments, rate constants were measured for each isoprene addition and for product release in the presence and absence of surfactant, and a kinetic model for the enzyme was developed (**Figure 5**).[19] This model displays FPP and IPP binding to UppS resulting in eight consecutive IPP condensations which afford the final C_{55}-BPP product. In the absence of Triton-X-100, both single and multiple turnover reactions afforded products longer than C_{55} with a very slow off-rate for the products (**Figure 5**). [19] However, in the presence of surfactant the C_{55} product was rapidly released and the rate limiting step of the reaction was changed from product release to the coupling of the second isoprene to FPP. [19] Steady-state measurements of UppS activity as described above would therefore be very difficult to interpret as they likely measure rates of the slowest step in the kinetic

mechanism, and interference of later steps could be invisible without monitoring product size.

In a single-turnover reaction, it was determined that Triton-X-100 can activate enzyme activity through acceleration post IPP condensation. A steady-state kinetics experiment determined that in the presence of 0.% surfactant, the $k_{cat} = 2.5\ s^{-1}$ was 190 times larger than without surfactant ($0.013\ s^{-1}$).[19,20] This indicated that the product-generating step in the absence of Triton-X-100 was not the limiting factor, but instead a subsequent step. In the presence of Triton-X-100, the single turn-over experiment suggested that the condensation of IPP was rate-limiting, not the release of product.[19]

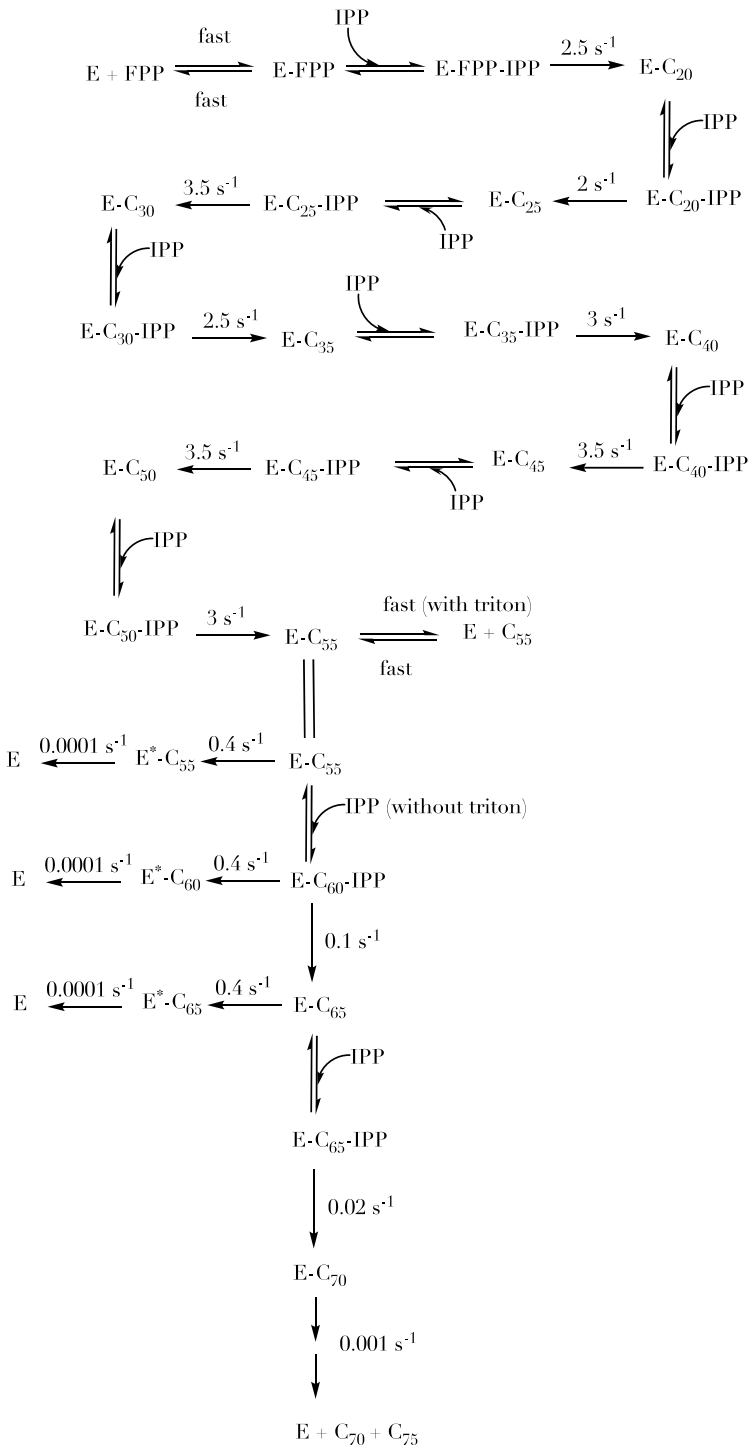

Figure 5*: Proposed kinetic pathway for UppS catalyzed reaction adapted from Liang et. al* [20]

Using both kinetic investigations and X-ray crystallography, Liang and coworkers also investigated the role of the metal ion in UppS catalysis. Reaction kinetics were determined using various concentrations of Mg^{2+}.[16] The binding of the homoallylic substrate requires the metal ion, however, too high of a Mg^{2+} concentration inhibits binding.[16] It was determined that the enzyme activity increases with increasing concentrations of Mg^{2+} from 0.02 to 1 mM, but then decreases substantially at a concentration of 50 mM.[16] The increase in activity with lower concentrations of $MgCl_2$ was attributed to the magnesium forming a complex with IPP.[16] FPP is able to bind to UppS without $MgCl_2$ present; however, IPP requires the metal ion.[16] Liang and coworkers proposed a catalytic mechanism in which FPP experiences electrostatic interactions and hydrogen bonding with Asn28, Gly29, Arg30, Arg39, and His43 (**Figure 6**).[16] This leads to a conformational change in UppS from "open" to "closed" conformations.[16] The Magnesium-IPP complex then hydrogen bonds with the nitrogen backbone atoms of Arg-194, Arg-200. Without residue Asp 26, the IPP would not be released from the magnesium complex.[16]

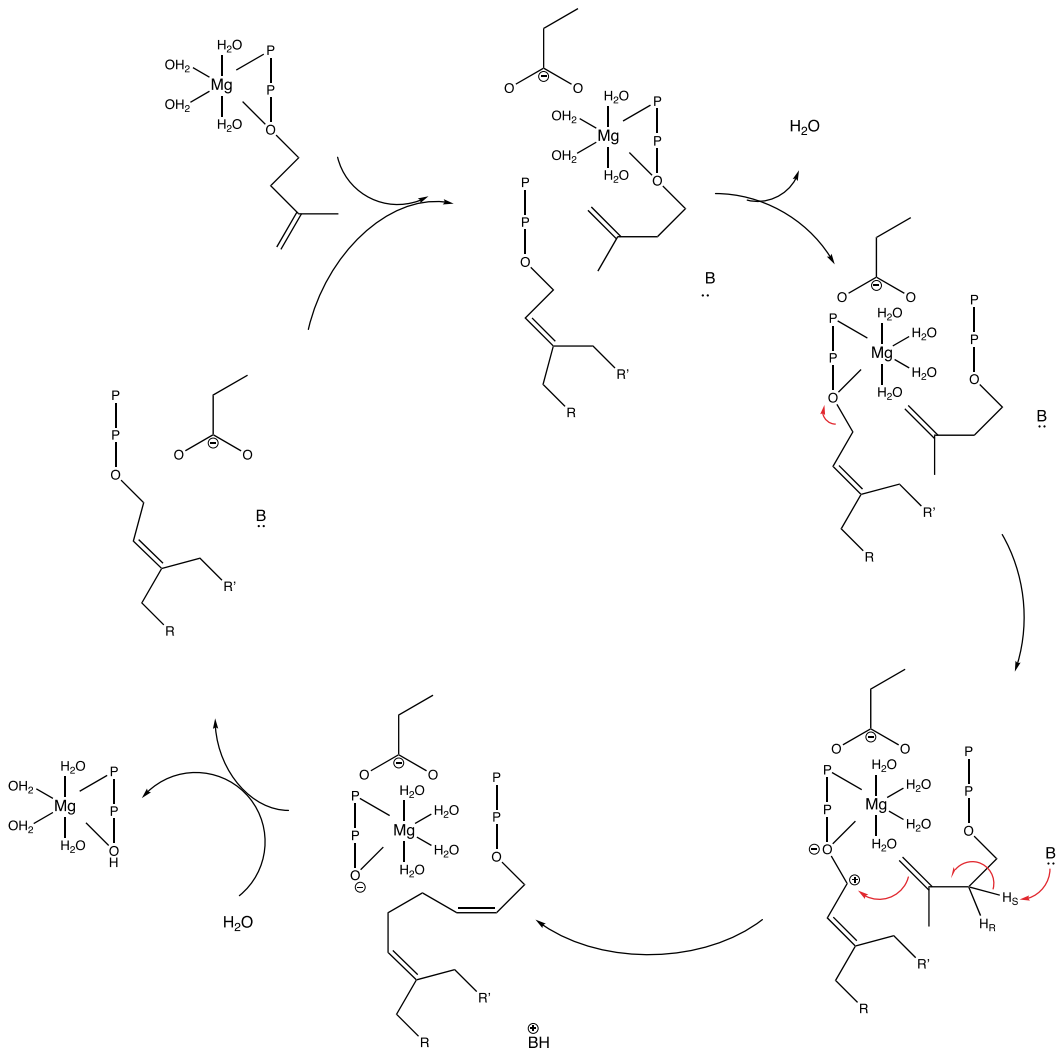

***Figure 6**: Proposed catalytic mechanism of UppS adapted from Liang et.al 2005*

1.2.2: UppS Inhibitors

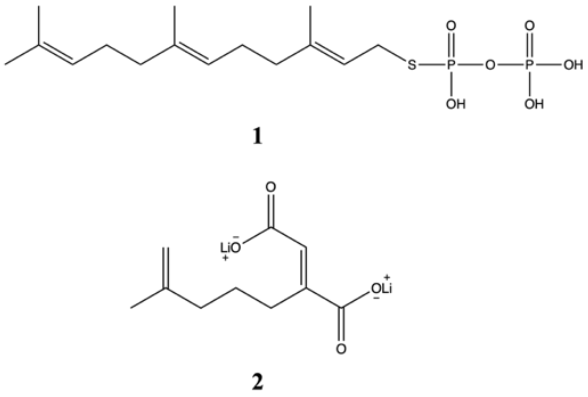

Figure 7*: Structures of UppS Inhibitors: (S)-Farnesyl thiopyrophosphate (FsPP) (1), and E-Pentenylbutanedioic acid (2)*

Since UppS is not produced by humans, developing inhibitors has been a goal for many researchers looking for an effective antibacterial agent.[21] In 2002, Chen et. al. synthesized (S)-Farnesyl thiopyrophosphate (FsPP) (**1**) as an alternative FPP analogue to probe enzyme activity.[15,22] FsPP contains a sulfur atom, replacing the oxygen atom in FPP that links diphosphate to the isoprenoid. This results in a non-hydrolysable FPP that can bind to isoprenoid-utilizing enzymes, but not react. FsPP was found to have an inhibitory effect on UppS from *E. coli* in *in vitro* enzyme assays with an enzyme IC_{50} value of 1.3 μM.[15]

To further explore UppS inhibition with isoprenoid structural analogues, a series of dicarboxylate isoprenoids were designed and synthesized.[12] The dicarboxylate was expected to mimic a diphosphate and serve as an inhibitor for the enzyme. Out of ten analogues synthesized and tested *in vitro* with UppS, only the trans dicarboxylate E-Pentenylbutanedioic acid (**2**) showed even modest inhibition against UppS, with an IC_{50} of 135 μM. The poor activity of these structural analogues was attributed to the potential

dependence on the specific shape or spatial arrangements of the diphosphate and isoprenoid.[12]

UppS inhibitors are likely to synergize with other cell-wall biosynthesis inhibitors, leading to potential decreases in antibiotic dosages and possibly restoring drug sensitivity.[21] Another notable study, reported on UppS inhibitors binding to one or more of four inhibitor binding sites that were identified computationally. This is significant due to the possibility of designing a more diversified scope of inhibitors.[21] Obtaining crystal structures of UppS from *E.coli* with benzoic, phosphonic, and diketoic acids, as well as cationic inhibitors, allowed the mechanism of how the inhibitors bind to their UppS target to be investigated. [21] Three of the binding sites occupy the top of the hydrophobic tunnel, whereas the fourth site is located at the bottom (**Figure 8**).[23]

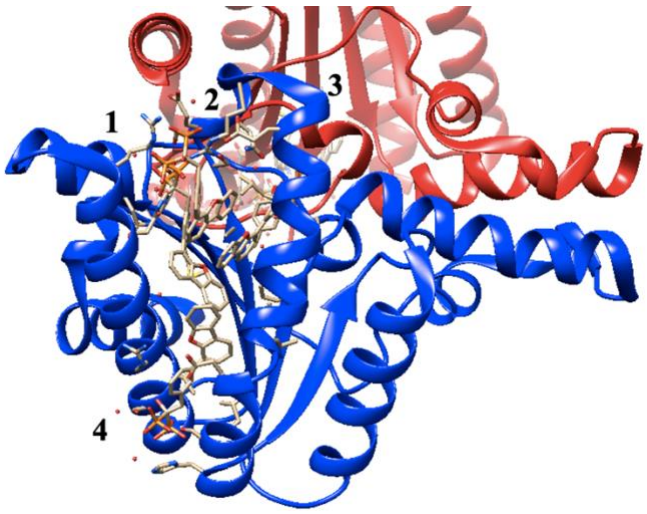

Figure 8*: UppS in complex with a bisphosphonate bound to sites 1-4 (PDB ID code 2E98)*

Binding site 1, near the top of the hydrophobic tunnel, is the main binding site of farnesyl diphosphate and includes residues R39, D26, N28, H43, and G29 (**Figure 8**).[13,16,23]

Binding site 2 is also located near the top of the tunnel, and is the main binding site of isopentenyl diphosphate. Binding site 2 involves residues S71, W75, R194, and R200.[13,16,23]Site 3 includes the positive R77 residue and hydrophobic F89 residue near the top of the tunnel. Binding site 4, located at the bottom of the tunnel, includes positively charged residues H103, R102, and R51.[21,23]The benzoic inhibitors were found in site 3 (PDB ID code 3SGT), but with relatively weak inhibitory behavior (IC_{50} = 150 μM) whereas, the bisphosphonate inhibitor was bound to sites 1-4 with a more potent IC_{50} value of 0.3 μM (**Figure 8**).[21]

Both anionic and cationic compounds surprisingly acted as UppS inhibitors. This was unexpected since the cationic compounds do not mimic the FPP substrate.[21] The cationic species had a "polar-hydrophobic-polar motif" where its polar, cationic groups were located at or near the protein's surface.[21] A correlation was found between the inhibitor potency and the binding to site 4, with the more potent inhibitors occupying site 4.[21] The biphenyl bisamidine was of particular interest due to its compelling activity against both UppS *in vitro* (IC50 = 0.1 μM) and methicillin-resistant *staphylococcus aureus* (MRSA) in cell assays (MIC90 = 0.25 $\mu g/mL$).[21]

Due to the rise of MRSA and other antibiotic resistant bacteria, inhibitors that target different enzymes within peptidoglycan synthesis are of major interest.[24,25] In 2014, McCammon used a combination of *in vitro* assays, cell based assay, and computational studies to develop new inhibitors of UppS. This study discovered three new inhibitor classes for UppS through computational screening against the ChemBridge EXPRESS compound library via a previously validated docking protocol (**Figure 9**).[24]

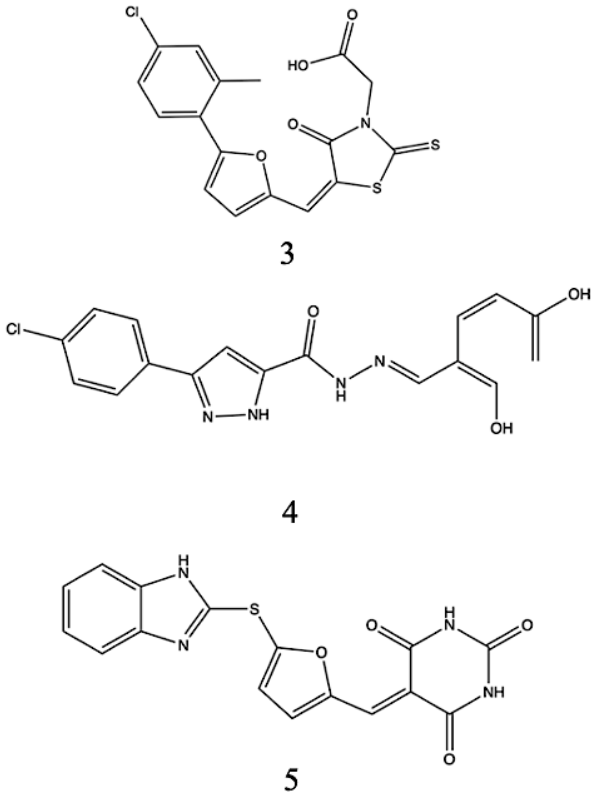

Figure 9*: Novel UppS inhibitor structures 3-5: rhodanines (3), dihydroxyphenyls (4), pyridinetrione (5)*

These novel UppS inhibitors included 4-oxo-2-thioxo-1,3-thiazolidines, or rhodanines (3), dihydroxyphenyls (4), and pyridinetrione (**5**) (**Figure 9**). Compound 3 is a rhodanine derivative that was determined to have a SaUppS IC_{50} value of 2.7 μM.[24] The resorcinol derivative (**4**) had an IC_{50} value of 13.7 μM against SaUppS, and the barbiturate compound had an IC_{50} value of 6.7 μM against SaUppS.[24] Each of these compounds likely bind to sites 1 or 3 (**Figure 8**). Due to the tendency of UppS inhibitors to concurrently bind to multiple binding sites, it is uncertain whether inhibitory activity is due to binding at one specific site or a result of multiple sites being occupied.[24]

1.3: Alternative substrate analogues for UppS

To study interactions between ligands and *E.coli* UppS, Liang et. al prepared a fluorescent analogue of FPP, [7-(2,6-dimethyl-8-phospho2,6-octadienyloxy)-8-methyl-4-trifluoromethyl-chromen-2-one] geranyl diphosphate or TFMC-GPP (**Figure 10C**).[26] This compound features the similar carbon skeleton as the natural substrate (FPP). It was demonstrated that the electron-withdrawing fluorinated substituent shifted the excitations/emissions to longer wavelengths, thus preventing interference from the protein's natural fluorescence.[26] The compound was found to have modest inhibitory behavior to FPP, with a (K_i =0.57 μM).[26]

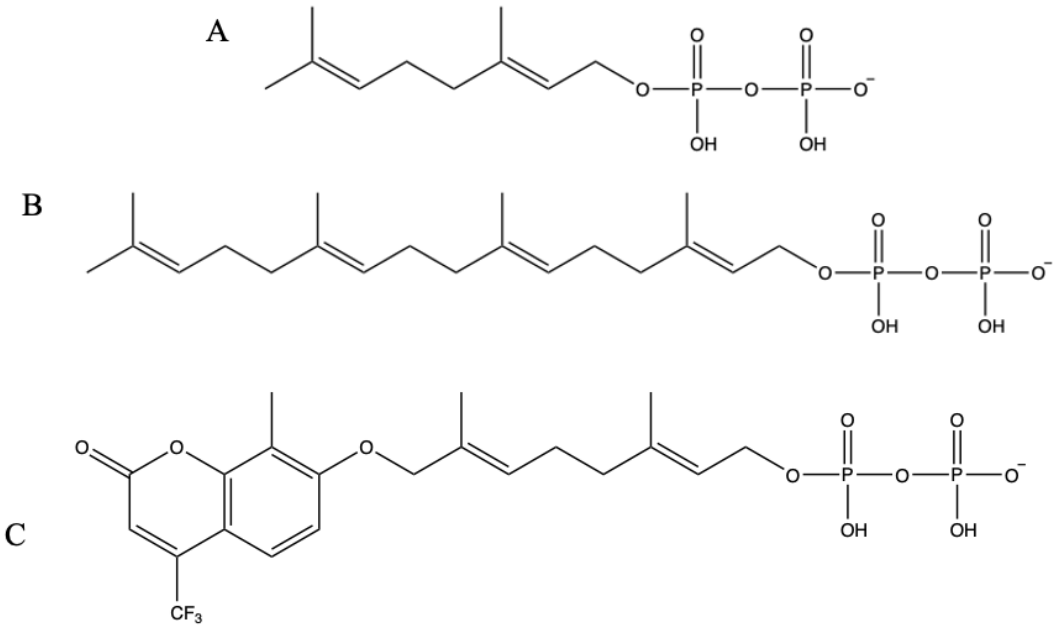

Figure 10*: Structures of alternative allylic substrates for UppS. A) C10-geranyl pyrophosphate. B) C20-geranylgeranyl pyrophosphate. C) [7-(2,6-dimethyl-8-phospho2,6-octadienyloxy)-8-methyl-4-trifluoromethyl-chromen-2-one]geranyl diphosphate or TFMC-GPP structure.*

To explore the impact of the hydrocarbon moiety of the allylic substrate FPP on the enzyme activity, kinetic studies utilizing all-trans geranyl pyrophosphate (C10-GPP), and Geranylgeranyl pyrophosphate (C20-GGPP) as alternative FPP substrates were formed (**Figure 10 A,B**). To examine the enzyme binding affinity, Liang and coworkers synthesized a monophosphate FPP analogue [7-(2,6-dimethyl-8-phospho2,6-octadienyloxy)-8-methyl-4-trifluoromethyl-chromen-2-one] or TFMC-GP to compare it to the native substrate (**Figure 10 C**).[26,18] The TFMC-GP incorporates "a fluorescent trifluoromethyl-chromen-2-one cross-linking to C10-GPP (geranyl pyrophosphate)."[18] It was determined that TFMC-GP bound to UppS acted as an inhibitor of FPP (K_i = 5.0 $\pm$ 0.3 μM). The C20-GGPP was determined to be a suitable alternative substrate (k_{cat} = 2.1 s^{-1} , K_m = 0.3 μM) for FPP.[18]

Po-Huang Liang and co-workers synthesized a novel FPP analogue with an appended chromen-2-one fluorophore for the investigation of ligand interaction with UppS (**Figure 11**) [26]. The fluorescent tag allowed the interaction study between natural FPP, and the FPP analogue with UppS.

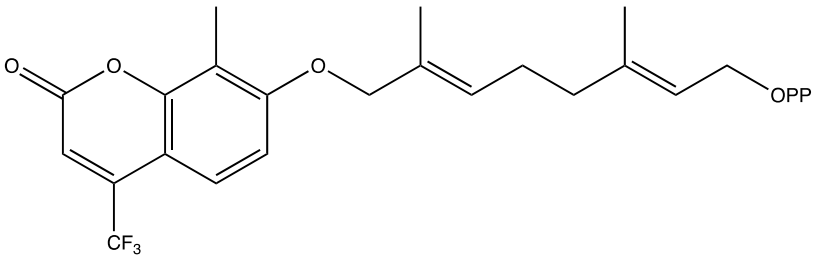

Figure 11*: Structure of FPP analogue possessing a chromen-2-one fluorophore*

It was found that the chromen-2-one fluorophore-tagged substrate worked as an alternative substrate only when the native FPP substrate was not present.[26] In the presence of native FPP, this fluorophore-tagged substrate acted as an inhibitor.[26]

In another study, Liang and coworkers synthesized a fluorescent analogue of FPP, (2E,6E)-8-O-(N-methyl-2-aminobenzoyl)-3,7-dimethyl-2,6-octan-dien-1-pyrophosphate (MANT-O-GPP) to see if the appended fluorophore to GPP would be elongated by UppS *E. coli* (**Figure 12**).[27] MANT-O-GPP was accepted as a substrate for UppS, and was successful in measuring enzyme kinetics.[27]

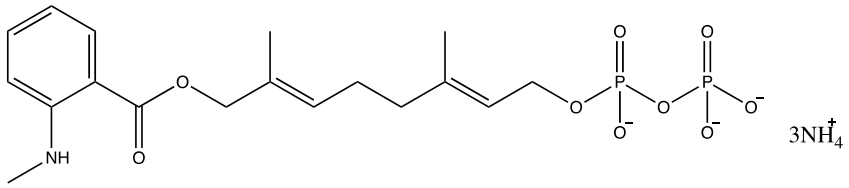

***Figure 12**: MANT-O-GPP structure*

When compared to FPP, MANT-O-GPP received one less isoprene addition, thus, indicating some steric hindrance of the MANT-O-GPP once it reached the bottom of the hydrophobic tunnel.[27] Ultimately, MANT-O-GPP was successfully elongated with 7 isoprene additions when incubated with UppS.[27]

1.3.1: Past Troutman-Lab Tags

In the past, our lab has synthesized various tagged geranyl diphosphates to be used as alternative substrates for UppS. Some of these tags include 2-amideanilinogeranyl diphosphate (2AA-GPP)[11], 2- nitrileanilinogeranyl diphosphate (2CNA-GPP)[11], and an ω-benzylazidogeranyl diphosphate (Az-GPP)[28] (**Figure 13**). It was found in 2013 that 2AA-

GPP was an accepted alternative substrate for UppS.[11] The results showed that 8 *cis* isoprene groups were able to be added.[11] Although this tag was successfully used as a substrate for UppS, it was only suitable for UppS from *B. fragilis* and was not particularly useful with UppS from *V. vulnificus* or *E. coli*.[11] This led us to search for a more universal tag that could be used. The Troutman lab has since synthesized tags that are capable of producing full-length 55-carbon long isoprene BPPs with a fluorescent tag. The 2CN-GPP tag was found to be fully functional with UppS from *E.coli*, *V.vulnifiucs*, and *B.fragilis*.[11] Using LC-MS selective ion mode (SIM) analysis, we found that Az-BPP products were also readily formed with 4-6 Z configuration isoprene additions (4-6Z, mimics C35-C45 BP)(**Figure 13).** Similar to 2CN, nitrobenzoxadizol (NBD) is a fluorescent probe that is known to be highly sensitive to its molecular environment (**Figure 13**).[29] This well-characterized fluorophore has also been used to develop a BP analogue for the investigation of isoprenoid-utilizing proteins.[30] The NBD-linked geranyl diphosphate is a suitable substrate for several proteins including UppS from *Bacteroides fragilis* ($UppS_{Bf}$), *Staphylococcus aureus* ($UppS_{Sa}$), and *Escherichia coli* ($UppS_{Ec}$).[30,2] Our results from this study suggest that subtle differences in the structures of these proteins could lead to an increase in activity with alternative substrate structures and vice versa.[30]

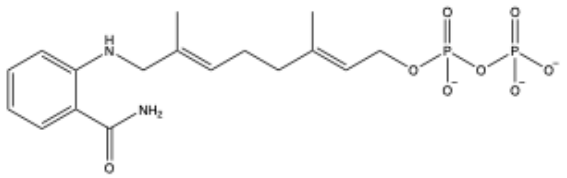

2AA-GPP

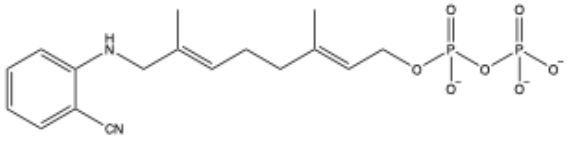

2CN-GPP

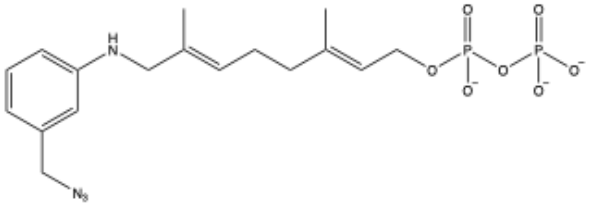

Az-GPP

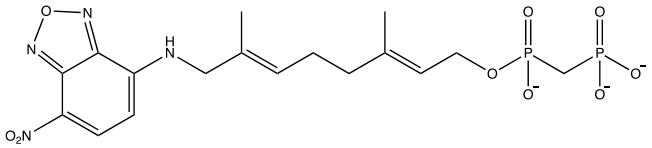

NBD-GPP

Figure 13*:* Molecular structures of Troutman lab alternative substrates. From top to bottom: 2-amideanilinogeranyl diphosphate (2AA-GPP), 2- nitrileanilinogeranyl diphosphate (2CNA-GPP), ω-benzylazidogeranyl diphosphate (Az-GPP), and nitrobenzoxadizol geranyl diphosphate (NBD-GPP).

1.4: The Role of FPP

Farnesyl diphosphate has an important role across kingdoms of biology and is the major product for the mevalonate pathway, which is crucial for almost all eukaryotic cells, as it is responsible for converting mevalonate into cholesterol.[31] The coupling of two FPP molecules affords squalene, which is a precursor to cholesterol formation.[32] The pathway of protein prenylation, inclusive of mevalonate production, was found to have connections to about 30% of all human cancers.[33] Protein prenylation catalyzed by protein farnesyl transferase is a post-translational modification that uses FPP to attach a farnesyl isoprenoid to cysteine residues in proteins.[33] Subsequently, enzymes in this pathway have become targets for potential therapeutics. When investigating an enzyme as a target for a possible therapeutic agent, it is important to take into account all possible cell-signaling pathways, as you may be dealing with more than one. Protein function is often an integrated function of a number of pathways to achieve a particular response.[9]

Due to its significance in a wide range of biology, isoprenoids like FPP have been a target for protein modification. Protein isoprenoid modification to probe enzyme function has been on the frontlines of research since the 1990s.[34] The extensive utilization of analogues to probe biological pathways resulted in a multitude of alternative FPP structures being produced. These analogues also provide a good launching point for the analysis of bacterial enzymes, including UppS. One class of probes worth mentioning are those that increase chemical functionalization using highly-selective bioorthogonal reactions which do not disrupt the system being studied.[35] These reactions have been extensively used in *in vivo* and *in vitro* experiments, for advances in probe technology, biomedical imaging, medicinal chemistry, materials science and polymer science.[35] While fluorophores are a

great tool for labeling, they generally do not have the sensitivity required for visualizing prenylated proteins in cellular extracts.[36] To increase the sensitivity, an alternative substrate tagged with a smaller functional group can be used. A biorthogonal reaction would allow the appendage of the labeling reagent. There have also been numerous synthetic analogues have been formed for use in prenylome studies. These labels used are commonly attached via a Cu-catalyzed alkyne-azide cycloaddition (CuAAC), or a Staudinger reaction.[37,38]

In 2005, Spielmann and coworkers formed an anilogeranyl FPP analogue (AGOH) with specific corresponding antibodies (**Figure 14**).[39] The AGOH analogue was successful in tracking enzyme activity in cells and modified cellular protein detection.[39]

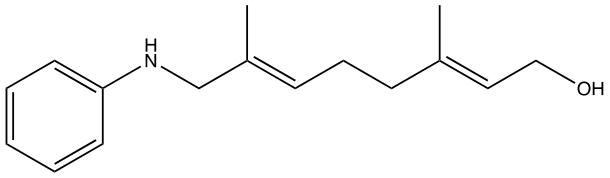

Figure 14*: FPP analogue AGOH structure*

AGOH can be utilized by a cell to modify proteins in a farnesyl transferase (FTase)-dependent manner.[39] The structure of the anilogeranyl moiety is unlike other known cellular components which is ideal for selective antibody recognition.[39] The corresponding antibodies formed were useful for screening both the activity and protein targeting of FTase inhibitors.[39] This aided in the identification of the reagent targets for the further investigation of farnesylated proteins in cancer biology.[39] One oncoprotein of particular interest is the GTP-binding Ras protein. This widely studied oncoprotein undergoes a post-translational modification at the carboxyl terminal end to achieve its biological activity.[40]

Step one in the 4-step modification is the attachment of 15 carbon farnesyl (FTase) to the cysteine residue.[40] Next, the cysteine-aliphatic-aliphatic-X (CAAX) Ras-converting endopeptidase 1 cleaves three terminal amino acid residues and the resulting isoprenylated cysteine residue is methylated by the isoprenylcysteine carboxyl methyltransferase (Icmt) as shown in **Figure 15.** [40,41,42]

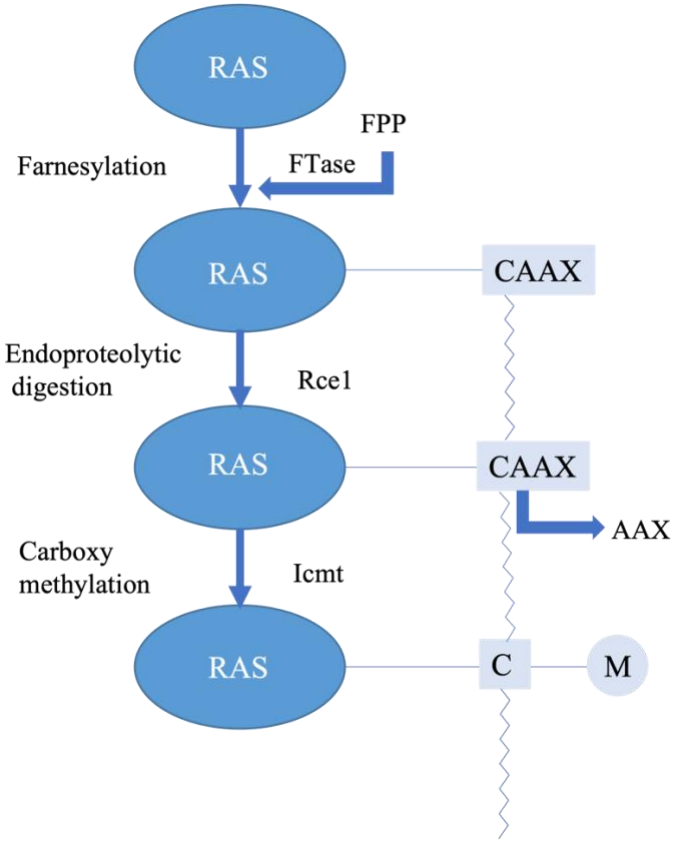

Figure 15*: Post translational modification in Ras oncoprotein occurring at the carboxyl terminal (CAAX)*

A study by Distefano and coworkers synthesized photoactive benzophenone-based analogues of FPP to identify amino acids in the active site of protein prenyltransferase to aid in the design of anticancer agents through the inhibition of the Ras oncoprotein.[43] These

benzophenone-based analogues are attractive for photoaffinity labeling experiments, as they are activated at a wavelength were protein damage is less likely. The photoaffinity labeling technique utilized in this study is highly useful for the investigation of interactions between substrates and enzymes.[43,44]

In 2006, a study by Spielmann and coworkers compared FPP analogue structures and their corresponding kinetics to probe the range of FPP modifications possible while still allowing efficient transfer by a farnesyl transferase (FTase), a prenyltransferase (**Figure 16**).[45,46] The first compound, 8-anilinogeranyl pyrophosphate (AGPP) was the building block of the photo-labeled compounds: 8-(p-nitro- anilino)geranyl pyrophosphate (NAGPP), and 6-(p-azido-N-methyl-tetrafluoro- anilino)-3-methyl-2-hexenyl pyrophosphate (MTAZA2PP). The second and third compounds were labeled with nitro-, and azide-aromatics respectively (**Figure 16**).[45]

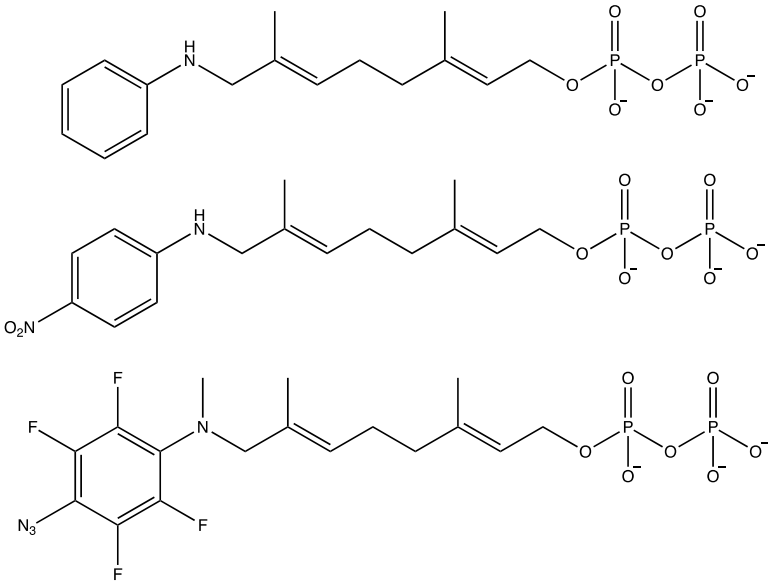

Figure 16*: FPP analogues: transferable FPP analogues 8-anilinogeranyl pyrophosphate (AGPP), 8-(p-nitro- anilino)geranyl pyrophosphate (NAGPP), 6-(p-azido-N-methyl-tetrafluoro- anilino)-3-methyl-2-hexenyl pyrophosphate (MTAZA2PP).*

It was found that ring fluorination and para substituents have little effect on the affinity of the analogue pyrophosphate for FTase and its transfer efficiency and were determined to be acceptable isoteres.[45]

To form an ideal biosynthetic probe, it is critical to understand the enzymes limitations on substrate modification. To further probe these limitations, our research group has formed several novel tags. After successfully synthesizing these FPP alternatives, there was still a need for analogues that would allow close investigation into the active site of the UppS enzyme. This could be done by slightly altering the size or shape of the tag used. This thesis aimed to investigate the specificity and selectivity of the UppS enzyme through the modification of the natural substrate farnesyl diphosphate (FPP) with carefully selected halogenated aromatics that test the selectivity of the enzyme based on size, electronegativity, and shape (**Figure 17**). The para-brominated FPP analogue was synthesized and utilized for enzymatic analysis of UppS *S.a.*

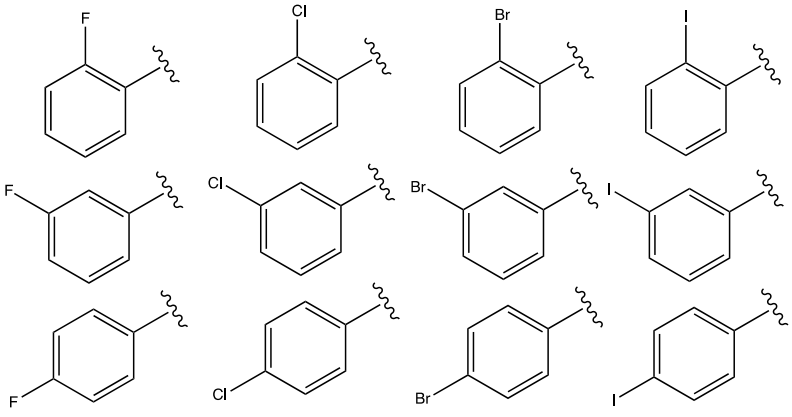

Figure 17: *FPP halogen-tagged analogues for the investigation of UppS enzyme activity*

CHAPTER 2: METHODOLOGY

2.1: Synthesis of halogenated geranyl diphosphate

*Synthesis of geranyl aldehyde (**1**)*

At 0ºC, 53.4 mL (0.554 mol) *tert*-ButylHOOH (70% aqueous), 75.0 mL dichloromethane, 1.1 g (0.010 mol) SeO_2, and 1.4 g (0.0010 mol) salicylic acid were added to a flask and stirred for 10 minutes. After 10 minutes, 20.0 grams of geranyl acetate (0.102 mol) was added and stirred for 5 hours. After this, the reaction was stirred at room temperature for an additional 18-20 hours.[47]

Next, 5% sodium bicarbonate was added. The solution was diluted with diethyl ether and extracted with brine. This was then washed with copper sulfate twice, sodium thiosulfate twice, and then a final rinse with brine. The resulting organic layer was then dried over magnesium sulfate for three minutes, filtered, and placed under vacuum to afford a crude geranyl aldehyde (**1**). The remaining oil was purified via flash chromatography. Thin layer chromatography (TLC) analysis was used to determine to column conditions. (POLYGRAM SIL G UV 254) TLC (30% EtOAc/Hexanes) R_f = 0.56. Silica flash chromatography was performed with 30% (v/v) ethyl acetate/hexanes solution. Yield: 16.8%, which is consistent with previously published yields.[2] 1HNMR (500MHz) 9.3 (s, 1H), 6.5 (t, 1H), 5.3 (t, 1H), 4.6 (d, 2H), 2.5 (td, 2H), 2.2 (t, 2H), 2.0 (s, 3H), 1.6 (s, 6H).

*Synthesis of halogenated geranyl acetate (**2**)*

Under argon, 0.5 g of pure geranyl aldehyde (**1**) (1 equiv.) and 12 mL of dichloromethane (1.2 equiv.) were added to a flame-dried flask. The solution was then stirred for two minutes and 0.0016 moles of each aniline (1.2 equiv.) was added. After

stirring the solution for 10 minutes, 1.0 g of sodium tri-acetoxy borohydride (2 equiv.) and 0.86 mL acetic acid (1.2 equiv.) were added. The solution was then stirred for 12-16 hours. After stirring, 5% sodium bicarbonate was added and allowed to stir at room temperature until effervescence ceased. This was then extracted with ether and brine. The collected organic layer was dried over sodium sulfate for three hours, and then placed under vacuum to afford a crude halogenated geranyl acetate (**2**). The remaining oil was purified via flash chromatography. Thin layer chromatography (TLC) analysis was used to determine to column conditions. TLC (30% EtOAc/Hexanes) $R_f = 0.8$. Silica flash chromatography was performed with 20% (v/v) ethyl acetate/hexanes solution. Yield: 52%, which is consistent with previously published yields.[2] 2BrGOAc: 1HNMR (500MHz) 7.2 (apparent doublet, 1H), 6.9 (ddd, 2H), 6.7 (ddd, 1H), 5.3 (t, 1H), 5.2 (t, 1H), 4.6 (d, 2H), 3.7 (apparent singlet, 2H), 2.3 (td, 2H), 2.1 (t, 2H), 2.0 (s, 3H), 1.7 (s, 6H). 3BrGOAc: 1HNMR (500MHz) 7.2 (apparent triplet, 1H), 7.1 (apparent triplet, 2H), 6.8 (dt, 1H), 5.4 (t, 1H), 5.2 (t, 1H), 4.6 (d, 2H), 3.7 (apparent singlet, 2H), 2.3 (td, 2H), 2.1 (t, 2H), 2.0 (s, 3H), 1.7 (s, 6H). 4BrGOAc: 1HNMR (500MHz) 7.2 (apparent doublet, 2H), 6.7 (apparent doublet, 2H), 5.3 (t, 1H), 5.2 (t, 1H), 4.6 (d, 2H), 3.7 (apparent singlet, 2H), 2.3 (td, 2H), 2.1 (apparent triplet, 2H), 2.0 (s, 3H) 1.7 (s, 6H).

*Synthesis of halogenated geranyl alcohol (**3**)*

In a 250 mL flask, 1.3 mmol of purified acetate (**2**) in excess methanol was stirred. 3.35 g (0.024 mol) of potassium carbonate dissolved in 7.5 mL of water was added to the solution and stirred for 12 hours at room temperature. The deacetylated product was then taken back up in ether, and washed with brine. The organic layer was dried over magnesium sulfate and then placed under vacuum to afford a crude halogenated geranyl alcohol (**3**).

The remaining oil was purified via flash chromatography. Thin layer chromatography (TLC) analysis was used to determine to column conditions. TLC (30 % EtOAc/Hexanes) $R_f = 0.48$. Silica flash chromatography was performed with 30% (v/v) ethyl acetate/hexanes solution. Yield: 80.7%, which is consistent with previously published yields.[2] 2BrGOH: 1HNMR (500MHz) 7.4 (apparent doublet, 1H), 7.12 (apparent triplet, 1H), 6.6 (d, 1H), 6.5 (t, 1H), 5.3 (t, 2H), 4.1 (apparent doublet, 2H), 3.6 (s, 2H), 2.0 (t, 2H), 2.15 (apparent triplet, 2H), 2.0 (t, 2H), 1.7 (s, 6H). 3BrGOH: 1HNMR (500MHz) 6.9 (apparent triplet, 1H), 6.76 (apparent doublet, 1H), 6.7 (apparent doublet, 1H), 5.36 (t, 2H), 4.09 (d, 2H), 3.57 (s, 2H), 2.15 (apparent triplet, 2H), 2.04 (apparent triplet, 2H), 1.7 (s, 6H). 4BrGOH: 1HNMR (500MHz) 7.2 (apparent doublet, 2H), 6.6 (apparent singlet, 2H), 5.3 (t, 2H), 4.13 (d, 2H), 3.62 (s, 2H), 2.15 (apparent triplet, 2H), 2.02 (apparent triplet, 2H), 1.7 (s, 6H).

*Synthesis of tris(tetra-n-butylammonium) diphosphate (**4**)*

A solution of 3.33 g (15.0 mmol) of sodium pyrophosphate dibasic in 15 mL of 10% (v/v) aqueous ammonium hydroxide was passed through a 2.5 X 7.0 cm column of Dowex AG 50W-X8 cation-exchange resin in HCl form.[48]The product was eluted with 110 mL of deionized water and was collected once a pH of 1.2 was reached, to a pH of 7. This was then immediately titrated to pH 7 with 40% (w/w) aqueous tetra-n-butylammonium hydroxide. The resulting solution was about 150 mL in total volume and was dried by lyophilization to yield a white hygroscopic solid. This was then purified by recrystallization through a cycle of drying twice with 75 mL of acetonitrile and then dried by rotary evaporation. The resulting solid was then warmed to 40 ℃ in 50–70 mL of ethyl acetate. Once heated, the solution underwent gravity filtration. The filtrate was reduced to 50%

volume through rotary evaporation and then cooled to approximately 8 ℃. The resulting crystals were washed with diethyl ether with typical recoveries between 35-50%. The purified crystals were taken up in acetonitrile to a concentration of 0.5 mg/mL.[48]

*Synthesis of halogenated geranyl diphosphate (**5**)*

Under argon, and to a flame-dried and cooled flask with stir bar, 0.5 mL of 100 mg/mL alcohol:dichloromethane solution (**3**) (1 equiv.) was added. To this, 0.15 mL of 1 M PBr_3 (0.75 equiv.) was slowly added. The reaction is immediately checked via TLC (30% EtOAc/hexanes) (R_f = 0.83) and then 3.0 mL of tris(tetra-b-butylammonium) diphosphate/acetonitrile (**4**) (TTNBAPP) (3-5 equiv.) for ion exchange, is added to the reaction. It was stirred for 30 min, and then checked via TLC (30% EtOAc/hexanes) (R_f = 0.78) again. The diphosphorylated product (**5**) was placed under vacuum to remove volatiles.

The concentrated reaction was then passed through AG® 50W-X8 ion-exchange resin in the ammonium form. The eluent was collected and lyophilized to yield a white hygroscopic solid. The halogenated diphosphate was then dissolved in 25 mM ammonium bicarbonate and purified by reverse phase HPLC monitored between 300 nm and 310 nm depending on the appended halogen. The purification utilized a gradient method with solvent A: 25 mM ammonium bicarbonate, solvent B: acetonitrile 0 min: 20% B, 20 min: 100% B. Preparative scale purifications were performed on a Varian Polaris C18-A 250 x 21.2 mm column at 2 mL/min. Yield: 15%. 2BrGPP ESI-MS (M-) expected: 482.01, 484.01 amu, Actual: 482.01, 484.01 amu. 3BrGPP ESI-MS (M-) expected: 482.01, 484.01 amu, Actual: 482.03, 484.03 amu. 4BrGPP ESI-MS (M-) expected: 482.01, 484.01 amu, Actual: 482.03, 484.03 amu. 2ClGPP ESI-MS (M-) expected: 438.06, 440.06 amu, Actual:

438.06, 440.06 amu. 3ClGPP ESI-MS (M-) expected: 438.06, 440.06 amu, Actual: 438.06, 440.06 amu. 4ClGPP ESI-MS (M-) expected: 438.06, 440.06 amu, Actual: 438.06, 440.06 amu.

2.2: Protein Expression and Purification of UppS *S.aureus*

A 5 mL starter culture of Luria-Bertani (LB) was prepared and was allowed to grow overnight. Terrific broth media, 20 g tryptone, 24 g yeast extract, glycerol 4 mL/L di H_2O, and 90 mM PBS solution.[2] The overnight culture was inoculated with 50 μg/mL kanamycin and then incubated at 37 °C at 220 rpm until an OD_{600} of approximately 0.6 was attained. 1 mM of Isopropyl β- d-1-thiogalactopyranoside (IPTG) was then added to the solution to induce overexpression. The culture was then incubated for 4 hours at 30 °C. After induction was completed, the media was removed from the cells through centrifugation at 10,000 g for 5 minutes at 4 °C. The cell pellets were then resuspended in 40 mL of lysis buffer, 50 mM Tris-HCl, 200 mM NaCl, and 20 mM Imidazole pH 8. The cells were then sonicated pulsing at 25% power for 3 minutes at 1 s on, 2 s off, for lysis.[2] The lysate was then centrifuged under a vacuum at 30,000 rpm for 1 hour at 4 °C. The resulting supernatant as poured onto a nickel affinity column containing approximately 2 mL of nickelnitrolotriacetic acid resin (Ni-NTA, PerfectoPro, 5 Prime Inc.) The lysate was passed through the column, collected, and then passed through again. Then, 25 mL of wash buffer (50 mM Tris-HCl pH 8.0, 200 mM NaCl, and 50 mM imidazole), was run through the nickel column. The protein was then eluted with elution buffer (100 mM Bicine pH 8.0, 200 mM NaCl, 50 mM KCl, 5 mM MgCl2, and 500 mM imidazole) and collected into 6 (1 mL) tubes. Analysis on all collected fractions (flow through, lysate, wash, and elutions)

was performed via SDS-PAGE gels to determine the fraction that contained the protein of interest.[2] A western blot was also performed using a second SDS-PAGE gel. The western blot was run at 30 V overnight at 4 °C. Elutions containing protein were combined and dialyzed three times in 1 L dialysis buffer (100 mM Bicine pH 8.0, 200 mM NaCl, 50 mM KCl, 5 mM MgCl2) at 4 °C with at least 4 h intervals in between buffer changes. The final concentrations, typically in excess of 500 μM, were calculated spectrophotometrically with an extinction coefficient of UppS *S. a* = 36,900 M^{-1} cm^{-1} .[2]

2.3: Chemoenzymatic Reaction

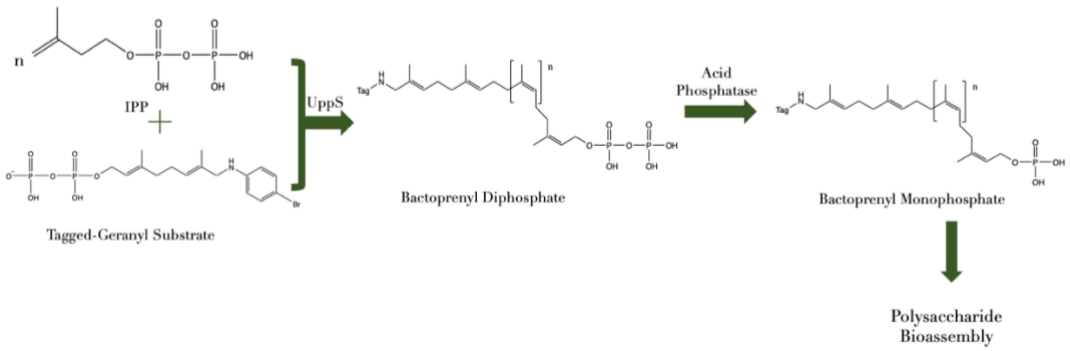

***Figure 18**: Chemoenzymatic synthesis scheme for producing a bromine-tagged bactoprenyl monophosphate*

Figure 18 depicts the chemoenzymatic synthesis scheme for the production of the bromine-tagged bactoprenyl monophosphate. The tagged FPP analogue (2.5 mM) and IPP (15 mM) are incubated for one hour with UppS (25 μM) along with 50 mM bicine, 5 mM potassium chloride, 0.5 mM magnesium chloride, and the surfactant, 2.4% octylthioglucoside (OTG), to yield bactoprenyl diphosphate analogue. After incubation,

the sample was then analyzed via LCMS to determine the number of isoprene additions using *m/z* values in **Table 1**.

Table 1*: Isoprene addition mass/charge ratios for chlorinated and brominated bactoprenyl diphosphates*

Isoprene Additions	**Chlorinated Bactoprenyl Diphosphates (*m/z*)**	**Brominated Bactoprenyl Diphosphates (*m/z*)**
0Z	438.06, 440.06	482.01, 484.01
1Z	506.13, 508.12	550.08, 552.07
2Z	574.19, 576.19	618.04, 620.04
3Z	646.28, 647.29	690.23, 692.23
4Z	711.32, 712.33	755.27, 757.27
5Z	779.38, 780.39	823.33, 825.33
6Z	847.45, 848.45	891.40, 893.39
7Z	914.50, 915.51	958.45, 960.45
8Z	982.56, 984.56	1026.51, 1028.51

Once the length of the BPP is determined, the terminal phosphate group was cleaved by the addition of acid phosphatase, to yield bactoprenyl monophosphate, the essential lipid carrier (**Figure 1**).

2.4: Purification Methods

2.4.1: Flash Chromatography

The flash chromatography column was packed with silica gel and hexanes. Once packed, the crude sample was slowly added to the top of the column using a Pasteur pipet. About 50-100 mL of additional hexanes was added to the column depending on column volume to ensure product/column interaction. To begin the separation by hydrophobic/hydrophilic interactions, a percentage of ethyl acetate in hexanes was added. This ratio varied depending on compound of interest (**Table 2**).

***Table 2**: Flash chromatography column conditions for halogenated acetate and alcohol elution*

Compound	% EtOAc/Hexanes needed for full elution
Brominated Geranyl Acetate	30
Chlorinated Geranyl Acetate	30
Brominated Geranyl Alcohol	50
Chlorinated Geranyl Alcohol	50

Fractions were collected and tested via TLC (30% EtOAc/hexanes) for product. This was continued up to 50 % ethyl acetate in hexanes if necessary for good separation.

2.4.2: High Performance Liquid Chromatography

Reverse phase HPLC was performed using a Varian C18 A250 x 21.1 mm column, and a Hewlett Packard Series 1100 absorbance detector. The mobile phase was a gradient mixture of 25 mM ammonium bicarbonate and acetonitrile depending on compound (**Table 3**).

***Table 3**: HPLC mobile phase gradients for brominated and chlorinated geranyl diphosphates*

Compound	% A: 25 mM Ammonium Bicarbonate	%B: Acetonitrile	Flow Rate (mL/min)
Brominated Geranyl Diphosphates	0 min: 80% 20 min: 0%	0 min: 20% 20 min: 100%	2.00
Chlorinated Geranyl Diphosphates	0 min: 85% 15 min: 80% 17 min: 0%	0 min: 15% 15 min: 20% 17 min: 100%	2.25

2.4.3: Cation Exchange Chromatography

Cation exchange was performed using Dowex AG* 50W-X8 cation exchange resin in the ammonium form (pH 7.8-8). The sample was eluted with 25 mM ammonium bicarbonate. The resulting solution was then lyophilized to afford the dried product.

2.4.4: Nuclear Magnetic Resonance Spectroscopy

All samples prepped for NMR analysis were taken up in deuterated chloroform ($CDCl_3$) and analyzed using a JEOL 500 MHz (JNM-ECA Series FT NMR) Nuclear Magnetic Resonance Spectrometer.

2.4.5: Liquid Chromatography Mass Spectrometry

ESI-LCMS was performed on an Agilent 1260 Infinity II LC System equipped with a single quadrupole. The column was a Waters C18 reverse phase column. Halogenated Geranyl Diphosphates: Mobile phase used was a gradient method with solvent A: 0.1% ammonium hydroxide, and solvent B: n-propanol 0 min: 5% B, 15 min: 90% B with a flow rate of 1 mL/min. Halogenated Bactoprenyl Diphosphates: Mobile phase used was a gradient method with solvent A: 0.1% ammonium hydroxide, and solvent B: n-propanol 0 min: 5% B, 22.50 min: 95% B with a flow rate of 1 mL/min.

CHAPTER 3: RESULTS AND DISCUSSION

3.1: Bromine Labeled Geranyl Diphosphate Synthesis Scheme

Figure 19 depicts the overall synthesis scheme for halogen-tagged geranyl diphosphates. Out of the halogens, bromine was chosen to be synthesized first due to the almost equally abundant bromine isotopes. The bromine isotope peaks appear at nearly equal abundance, two *m/z* units away at 482.01 *m/z* and 484.01 *m/z*. Bromines molecular ion ^{79}Br makes up 51% and its' isotope, ^{81}Br contributing 49% of natural abundance.[49] These isotopes allowed the bromine-appended molecules to be easily identified using mass spectrometry. Chlorine is also readily recognized on a mass spectrum due to its isotope where 76% of chlorine molecules exist as ^{35}Cl, and 24% of ^{37}Cl.[50]

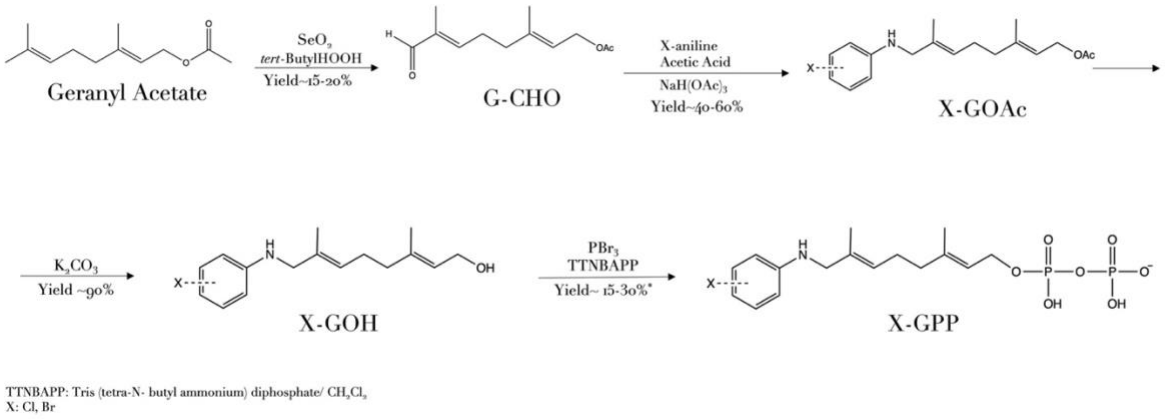

***Figure 19**:Halogenated Geranyl Diphosphate Synthesis Scheme*

These easily characterized compounds specifically, were selected with this in mind to then study the active site of UppS. The brominated set was investigated first, and included: 2-bromoaniline, 3-bromoaniline, and 4-bromoaniline appended to geranyl diphosphate. The chlorine set was second, and included: 2-chloroaniline, 3-chloroaniline,

4-chloroaniline. These easily characterized compounds specifically, were selected with this in mind to then study the active site of UppS.

The first step of the synthesis was adapted from Dodbele et. al. and began with geranyl acetate in which selenium dioxide and *tert*-butyl hydroperoxide were added to afford geranyl aldehyde (15-20% yield), along with both geranyl alcohol, and geranyl carboxylic acid.[11] The crude product was then purified via flash chromatography with a ethyl acetate:hexanes mobile phase. The pure geranyl aldehyde then underwent reductive amination. Initially, this step included $TiCl_4$ and pyridine to accelerate the reaction, though when applied to this study, it was found to be unsuccessful. This was attributed to the extreme water sensitivity of $TiCl_4$. Although the reaction was completed under inert gas, it is suspected that the $TiCl_4$ degenerated due to the inability to safely flame-dry the flask beforehand. Another factor hindering this reaction could have been pyridines sensitivity to light, as this reaction was attempted in a light-filled environment for several hours. Therefore, a method change was deemed necessary. The next reductive amination reaction attempted, began with the addition of the choice aniline to the aldehyde (**1**) along with glacial acetic acid, and sodium triacetoxy borohydride ($NaBH(OAc)_3$) producing the tagged-geranyl acetate (40-60% yield). The mild reducing agent, $NaBH(OAc)_3$ was selected instead of conventional reducing agents such as $NaCNBH_3$/MeOH and BH_3-pyridine, to achieve higher yields with fewer side products.

The crude tagged-geranyl acetate (**2**) was purified by flash chromatography and characterized by TLC before moving on to the next step. Once purified, the halogenated geranyl acetate (**2**) was deacetylated via potassium carbonate and purified through flash chromatography. The halogenated geranyl alcohol (**3**) product was then diphosphorylated

via phosphorous tribromide and tris [tetra-N-butyl ammonium] diphosphate (**4**) to achieve the tagged-geranyl diphosphate (**5**) (15-30% yield). After the addition of the phosphorous tribromide, the reaction had to be immediately checked via TLC to ensure the alcohol was consumed**.** Once TTNBAPP was added and the reaction was completed, it was checked again. The brominated intermediate spot was expected to decrease greatly in size, while the diphosphate spot was to appear around the baseline of the plate**.** However, this signal often did not drastically decrease even with the new appearance of the diphosphorylated product. The diphosphorylated products were further examined via mass spectrometry to verify the success of the reaction. It was determined that although the brominated intermediate remained on the TLC plate for the final product, the reaction still produced geranyl diphosphate.

Previous methods of producing allylic diphosphates involved treating the alcohol with inorganic phosphate and trichloroacetonitrile.[51] The allylic diphosphate had to then be isolated through ion-exchange chromatography from a mixture of inorganic and organic mono-, di-, and triphosphates.[51] To bypass these issues, the carbon-oxygen bond was introduced in the final step using an inorganic diphosphate salt, tris [tetra-N-butyl ammonium] diphosphate was employed.[52] The halogenated geranyl alcohol was first converted into a brominated intermediate that was capable of undergoing a displacement. An aprotic solvent was needed to avoid solvolysis, and therefore acetonitrile was chosen.

This method was fraught with difficulties due to the lengthy synthesis of TTNBAPP, which had to be synthesized in-house. One issue was the determination of pH during cation exchange. Initially, the pH was determined using Fisherbrand Paper pH

strips, and therefore only approximate pH could be determined. To get a closer approximation, the pH strips used were switched to MilliporeSigma™ MQuant™ pH Test Strips. The method dictated that the elution of free acid with 110 mL began once a pH of 1.2 was reached.[48] This drastic drop in pH occurred rapidly and was difficult to detect without un-interrupted real time pH analysis. Following ion-exchange, the solution had to be lyophilized. This often took one to two days due to the amount of product, as well as lyophilization instrument used. During crystallization of the TTNABPP, the method stated to allow crystallization overnight at -20 °C, however, this temperature did crystal generated even after 3 days.[48] After re-preparation, crystallization was attempted at a higher temperature of 4 ℃ and was successful.

The syntheses of the halogen-appended geranyl acetates proved to have their own difficulties. It was found that the yields for the ortho positioned halogen-tagged geranyl acetates had the lowest intermediate and final-product yields. This was unexpected since the synthesis procedure was adapted from our previous research which synthesized 2CN-GPP, where the formation of the acetate yielded (57%) versus the 2BrGPP in this study, which yielded an average of 29%.[2] To circumvent the low yields in the initial reductive amination steps of the ortho-labeled analogues, the synthesis reagents were all doubled and resulted in a sufficient amount of purified product to continue the following steps.

3.2 Alternative FPP analogue synthesis and characterization

Before the diphosphorylation step, the halogenated-alcohol intermediates had to be purified and characterized. Obtaining an accurate weight of the geranyl diphosphates was problematic due to the scale of the diphosphorylation reaction. The larger scale of the

tagged-geranyl alcohol synthesis allowed for the weighing of the purified product. Therefore, the molar absorptivity's of the alcohols were calculated in order to determine the concentrations of the diphosphates based on the presence of aromatics. The molar absorptivity for the brominated geranyl alcohols (**Figure 20**) was calculated using the Beer-Lambert law (**Equation 1**).

Equation 1: $A = \varepsilon C l$

The molar absorptivity's and corresponding maximum absorbance wavelengths (λ_{max}) for the chlorinated and brominated geranyl alcohols are found in **Table 4**.

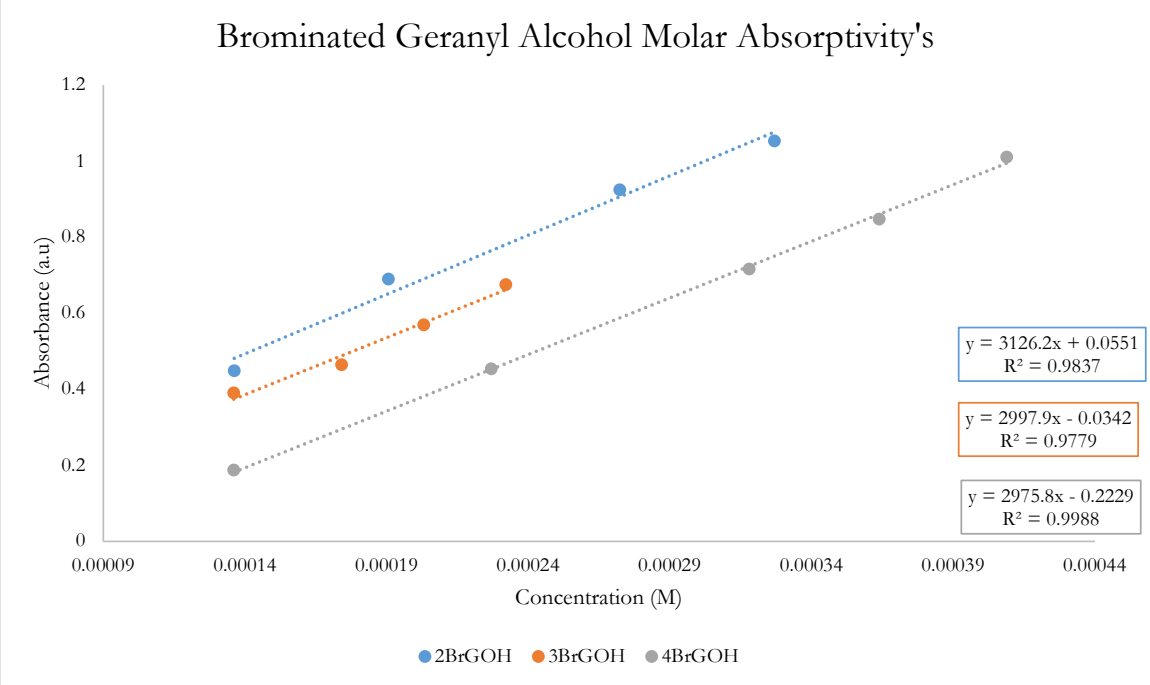

***Figure 20**: Brominated geranyl alcohol molar absorptivity's*

The molar absorptivity's for the brominated geranyl alcohols had an average extinction coefficient of 2968 $M^{-1}cm^{-1}$, and an average maximum absorbance wavelength

(λ_{max}) of 306 nm (**Table 4**). The molar absorptivity's for the chlorinated geranyl alcohols were, as expected, quite similar to the brominated geranyl alcohols. Chlorinated geranyl alcohols had an average molar absorptivity of 1497 $M^{-1}cm^{-1}$ (**Figure 21**), and an average maximum absorbance wavelength (λ_{max}) of 305 nm (**Table 4**).

***Table 4**: Maximum absorbance wavelengths and corresponding extinction coefficients for halogenated geranyl alcohols*

Halogenated Geranyl Alcohols	Maximum Absorbance Wavelength (nm)	Extinction Coefficient ($M^{-1}cm^{-1}$)
2BrGOH	310	2945.5
3BrGOH	300	3310.7
4BrGOH	310	2648.8
2ClGOH	300	3032.6
3ClGOH	306	2284.4
4ClGOH	310	2205.1

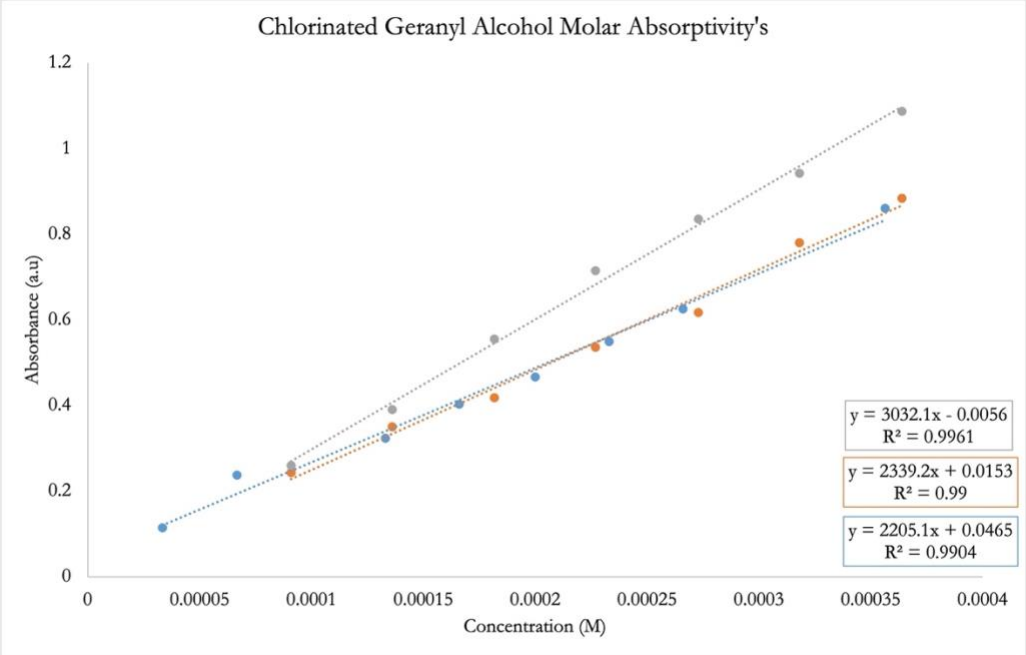

***Figure 21**:Chlorinated geranyl alcohol molar absorptivity's*

Once purified by flash chromatography, the halogenated geranyl alcohols were analyzed via HNMR in $CDCl_3$. For 2BrGOH, the HNMR spectrum is found in **Figure 23**. The four hydrogens H_A, H_B, H_C, and H_D, on the aromatic ring of 2BrGOH are accounted for in the aromatic region between 6.5 ppm and 7.5 ppm. H_A is a doublet of doublets of doublets (ddd) at 7.4 ppm, H_B and H_C are accounted for between the two peaks at 6.58 and 7.12 ppm as doublets. The last aromatic hydrogen H_D is a triplet located at 6.76 ppm. H_G and H_L are accounted for in the apparent triplet at 5.3 ppm. The group of H_M hydrogens appears at 4.1ppm as an apparent doublet. H_E hydrogens appear slight up field of H_M as a singlet at 3.6 ppm. H_I hydrogens are accounted for in the apparent triplet at 2.15. The peak for H_I also contains an ambiguous hydrogen. This is thought to be the hydroxyl proton (H_N). The H_J hydrogens appear at 2.0 ppm as an apparent triplet. The two methyl group hydrogens H_F and H_K are observed at about 1.6 ppm in the form of two singlets.

As expected, the HNMR spectrum for 3BrGOH (**Figure 24**) is similar to the spectrum for 2BrGOH,as the structure of the geranyl chain is identical. The key difference between the two spectra exist in the aromatic region. For 3BrGOH, H_B is most likely the peak at 6.7 ppm as a ddd. H_A is most likely at 6.76 ppm, while H_C is a triplet of doublets (td) at 6.96 ppm, and the last aromatic hydrogen, H_D, is accounted for in the peak at 6.4 ppm. The HNMR spectrum for 4BrGOH is found in **Figure 24** below. While the up-field of the spectrum remains widely unchanged in comparison to 2BrGOH and 3BrGOH spectra, the aromatic region has slight changes to note. Aromatic hydrogens H_A and H_D are accounted for in the signal at 6.69 ppm. The last two aromatic hydrogens H_B and H_C are represented by the signal at 7.26 ppm.

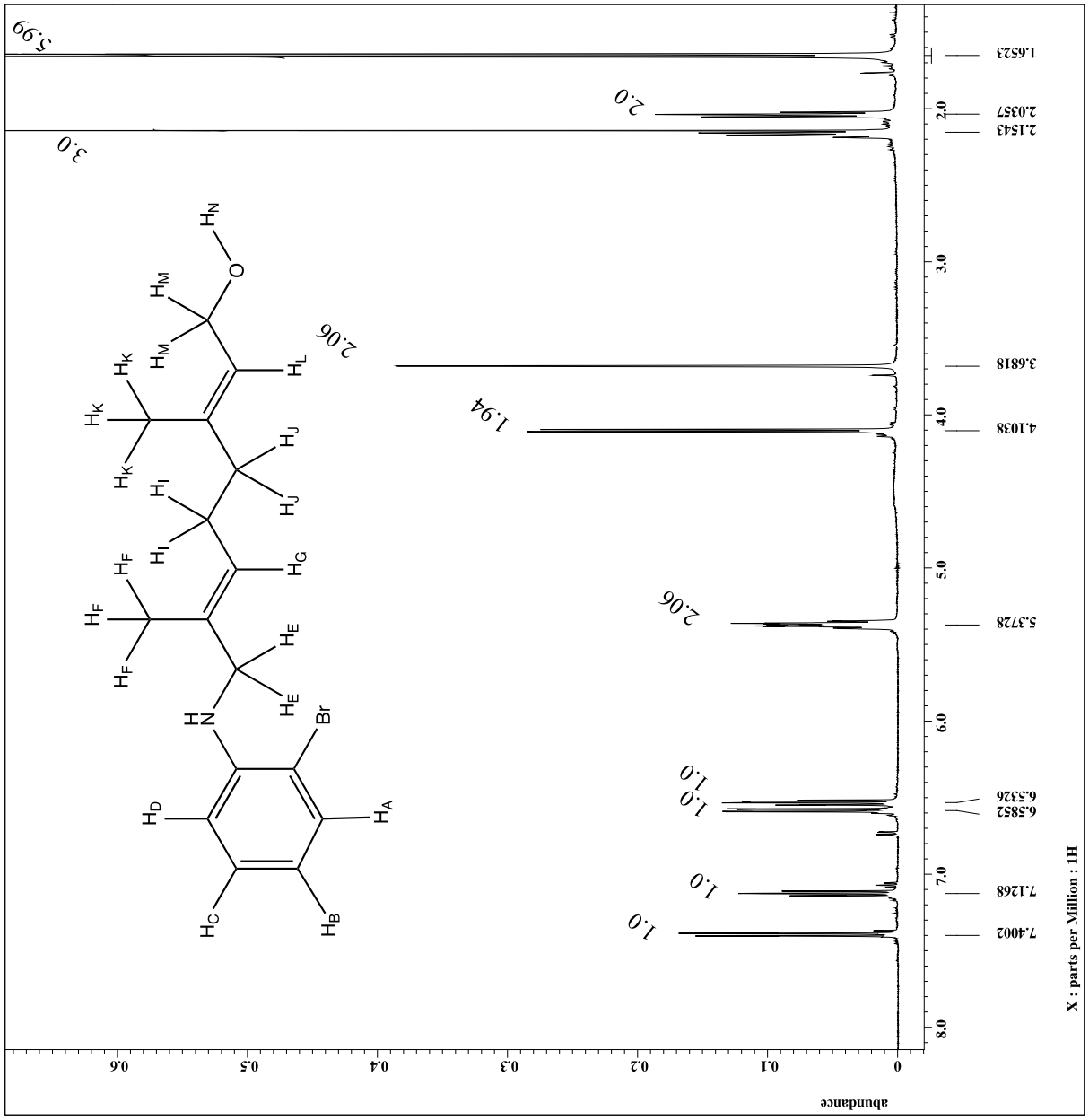

Figure 22: *2BrGOH HNMR spectrum with structure overlay*

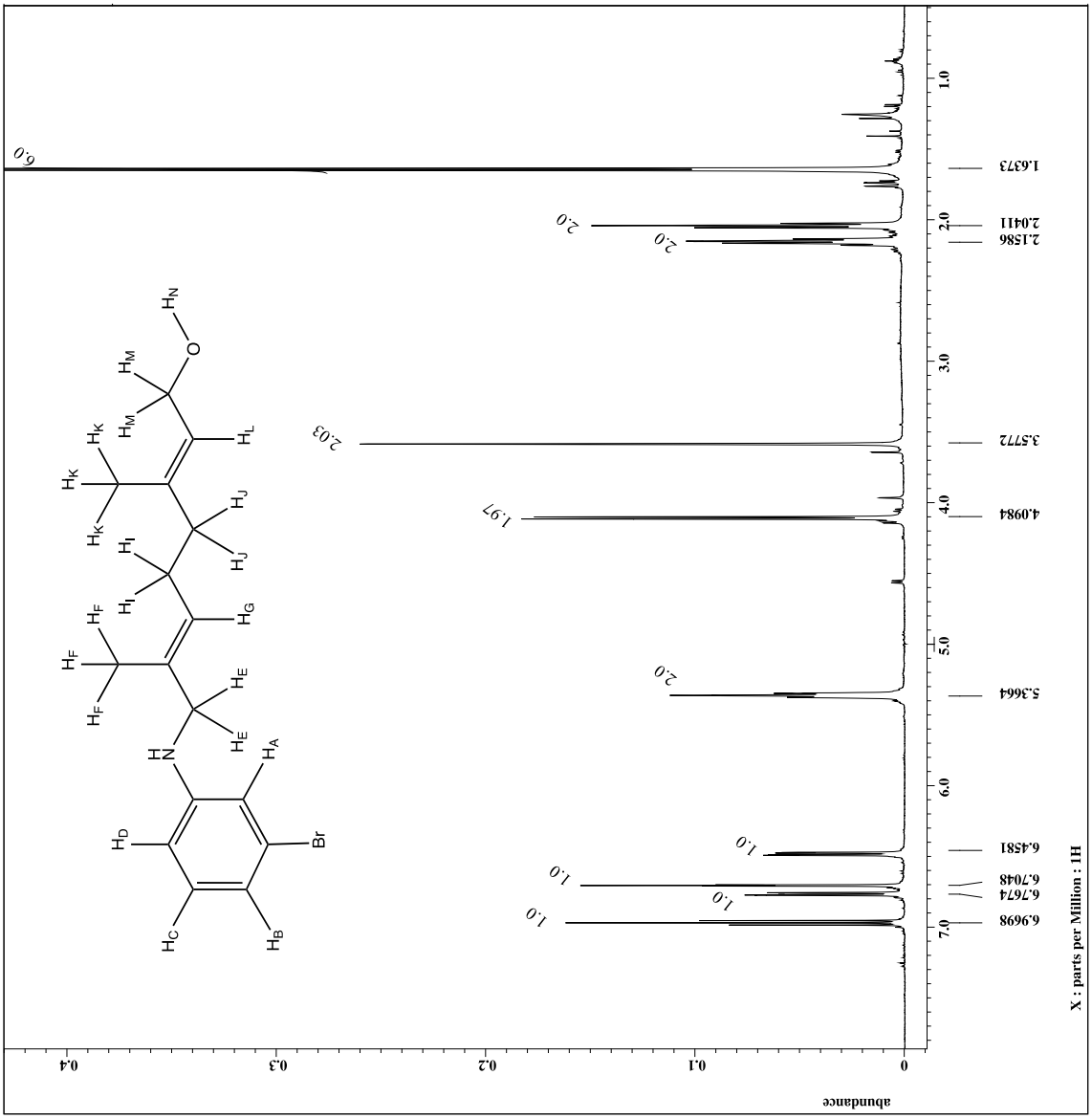

***Figure 23**: 3BrGOH HNMR spectrum with structure overlay*

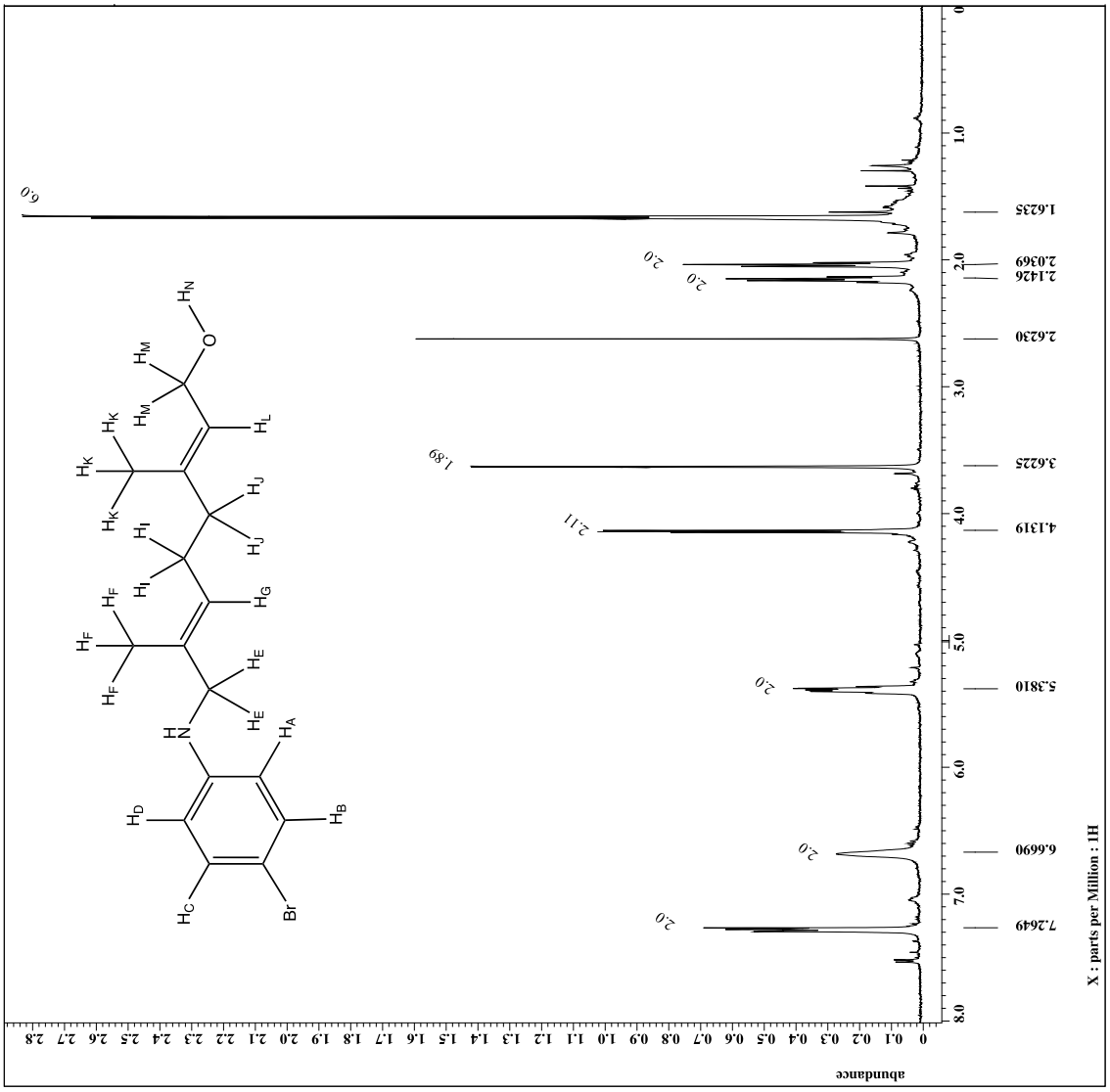

***Figure 24**: 4BrGOH HNMR spectrum with structure overlay*

The HNMR spectrum for 2ClGOH can be found in **Figure 25**. As expected, the downfield region of the spectrum is practically unchanged. Up-field, the aromatic hydrogen H_A appears at 7.25 ppm as a doublet, aromatic hydrogen H_B is accounted for in the signal

at 6.64 ppm along with H_D and finally, H_C is represented by the triplet signal at 7.01 ppm. Likewise, 3ClGOH (**Figure 27)** is comparable to the 3BrGOH spectrum with the key differences in the aromatic region. H_A, is represented in the signal at about 7.1 ppm, H_B likely produced the signal at about 6.6 ppm, and the other 2 aromatic hydrogens H_D and H_C are represented by the signal at 6.65 ppm. The HNMR spectrum for 4ClGOH shows H_A and H_D accounted for under the signal at 6.6 ppm, and H_B appears with H_C in the signal located at 7.1 ppm (**Figure 27**). This is shifted slightly up-field when compared to the 4BrGOH.

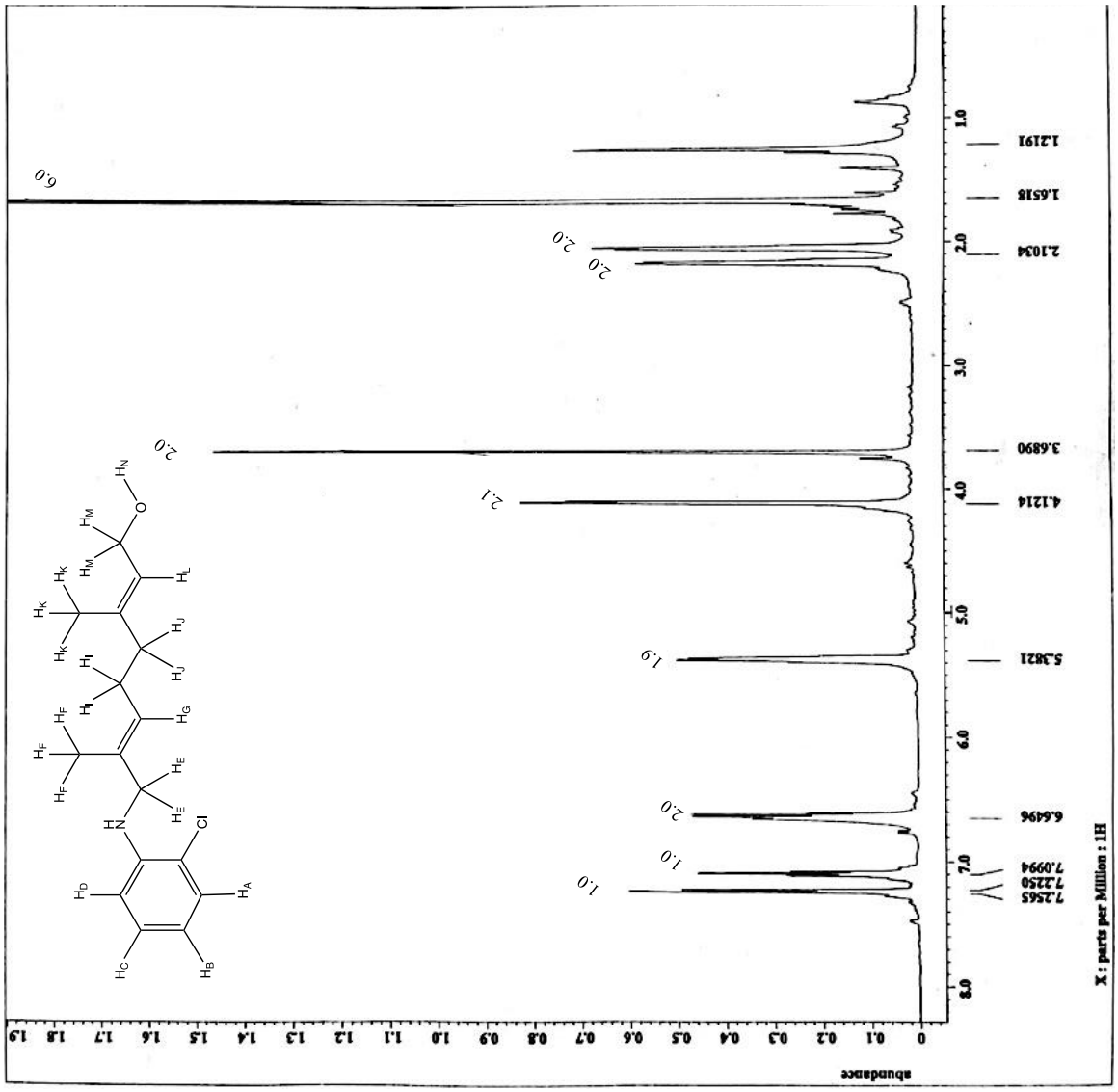

***Figure 25**: HNMR spectrum of 2ClGOH with structure overlay*

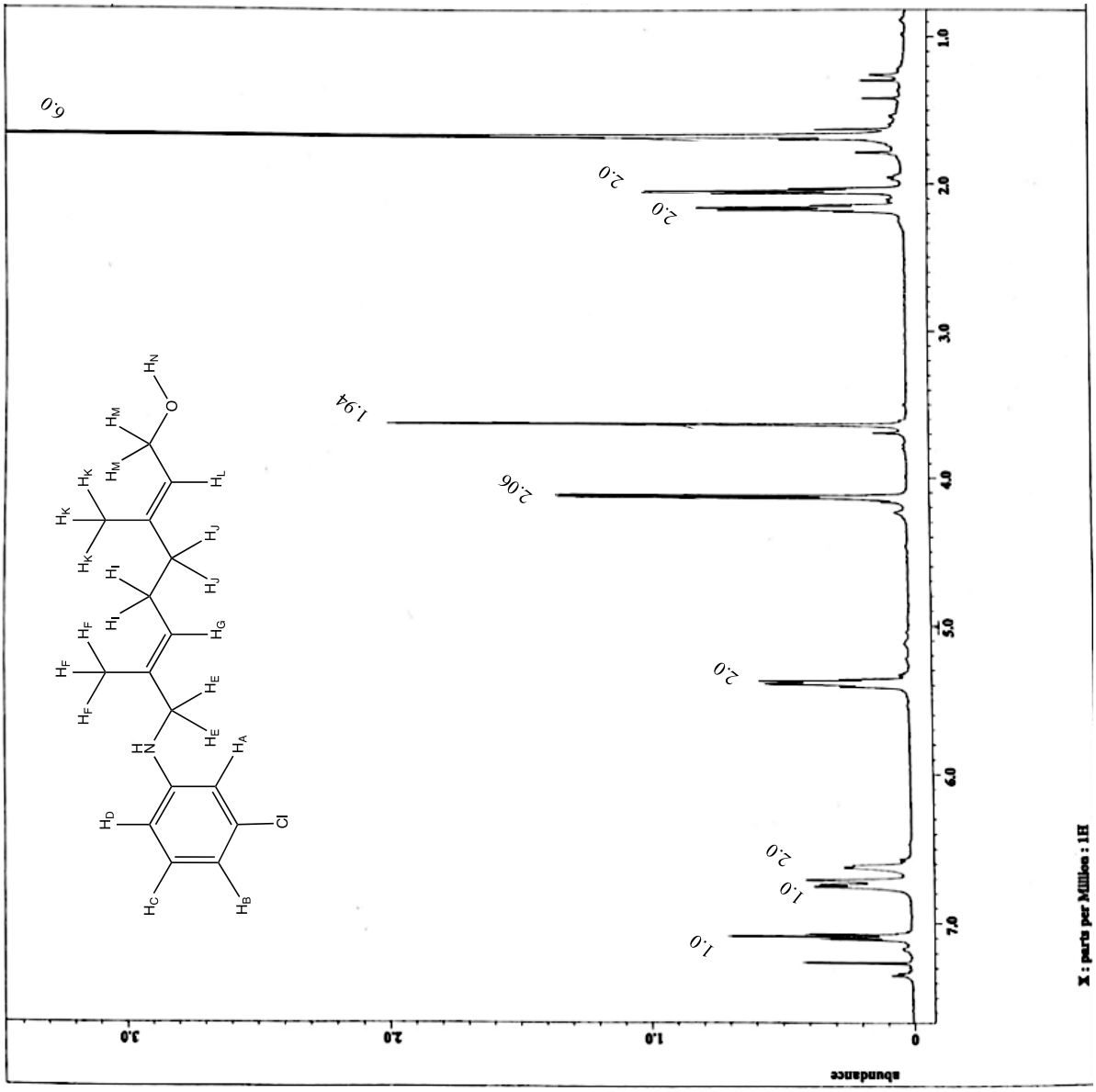

***Figure 26**: HNMR spectrum of 3ClGOH with structure overlay*

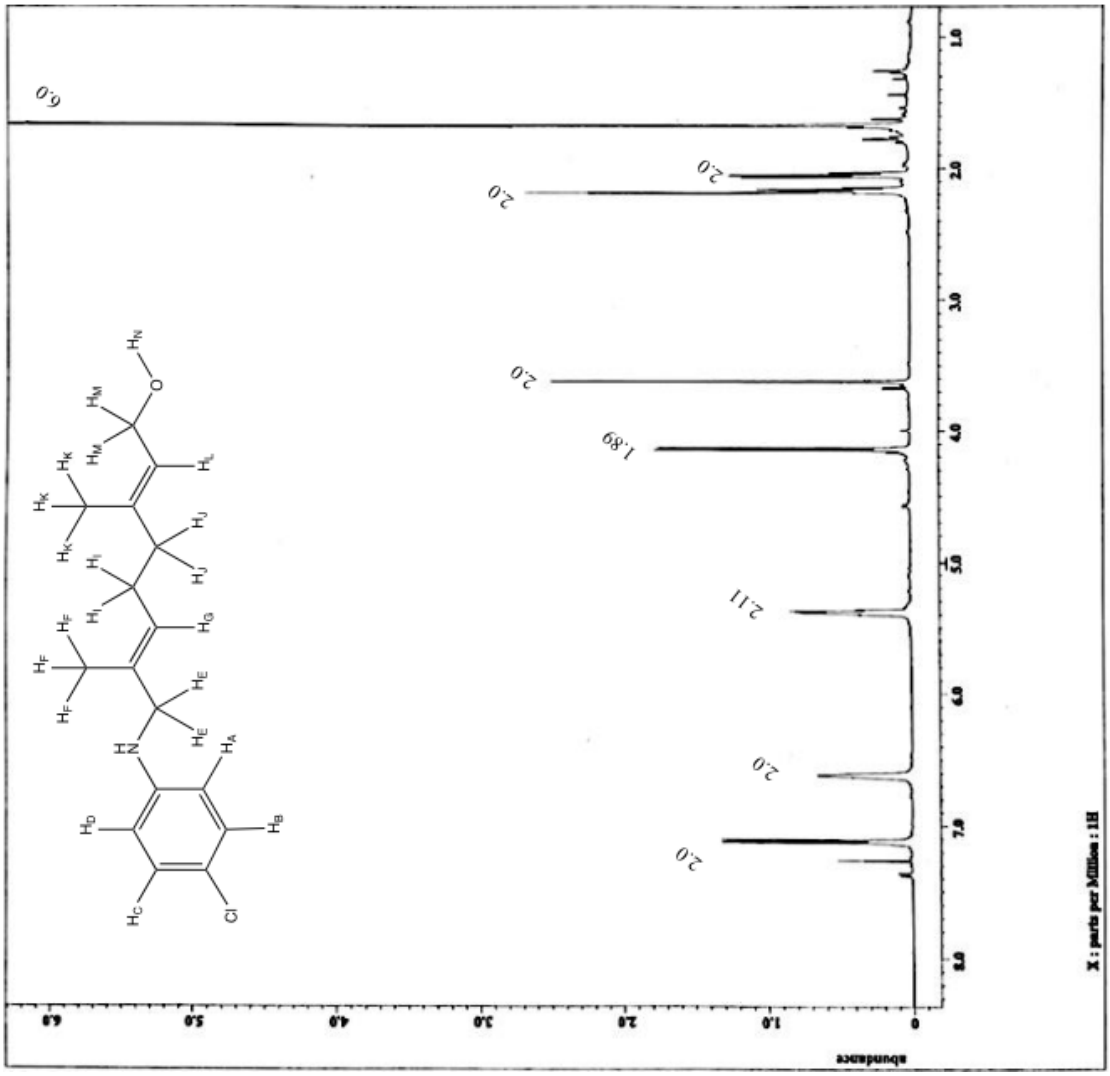

Figure 27: *HNMR spectrum of 4ClGOH with structure overlay*

The brominated and chlorinated sets of geranyl diphosphates were successfully synthesized and characterized via LCMS. The mass spectrum for 2BrGPP (**Figure 28)** shows two almost equally abundant peaks separated by two mass units at 482.01 *m/z* and 484.01 *m/z*. Similarly, 3BrGPP had the same two signature peaks at 482.01 *m/z* and 484.01

m/z (**Figure 29**). The bromine peak and the M+2 peak for 4BrGPP were shifted slightly to the right with *m/z* values of 482.03 *m/z*, and 484.03 *m/z* (**Figure 30**).

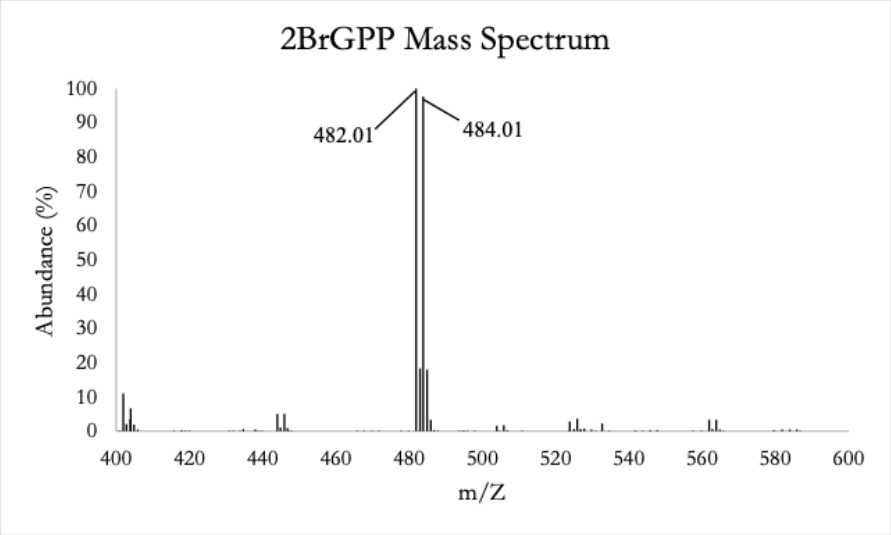

Figure 28: *Mass spectrum for 2BrGPP*

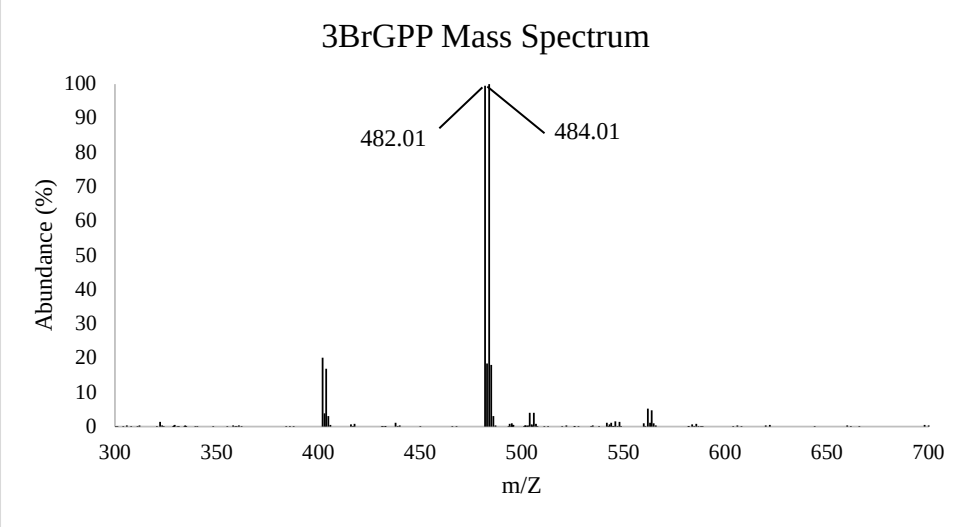

Figure 29*: Mass Spectrum for 3BrGPP*

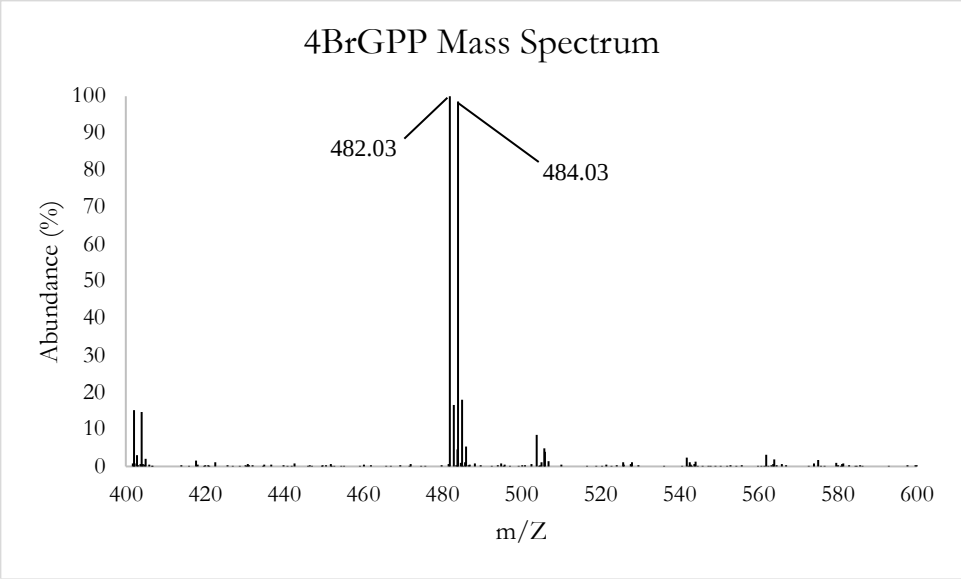

***Figure 30**: Mass Spectrum for 4BrGPP*

The expected signals from the chlorinated compounds were consistent with the data collected. For 2ClGPP, the mass spectrum shows a signal at 438.06 *m/z* with approximately 98% abundance and a signal at 440.06 *m/z* with approximately 38% abundance (**Figure 31**). Also noteworthy are the two peaks at 876.12 *m/z* and 880.12 *m/z*. These peaks are most likely dimers of the two isotopes of 2ClGPP. The 3ClGPP mass spectrum also had two signals at 438.06 and 440.06 *m/z* with similar abundances compared to 2ClGPP signals (**Figure 32**). The dimer signals for this chlorinated diphosphate was also observed with an even larger abundance than seen with 2ClGPP. Likewise the mass spectrum for 4ClGPP displayed two signals at 438.06, and 440.06 *m/z* with similar abundances compared to 2ClGPP signals (**Figure 33**). The dimer signals for this chlorinated diphosphate were observed with a similar abundance as seen with 2ClGPP.

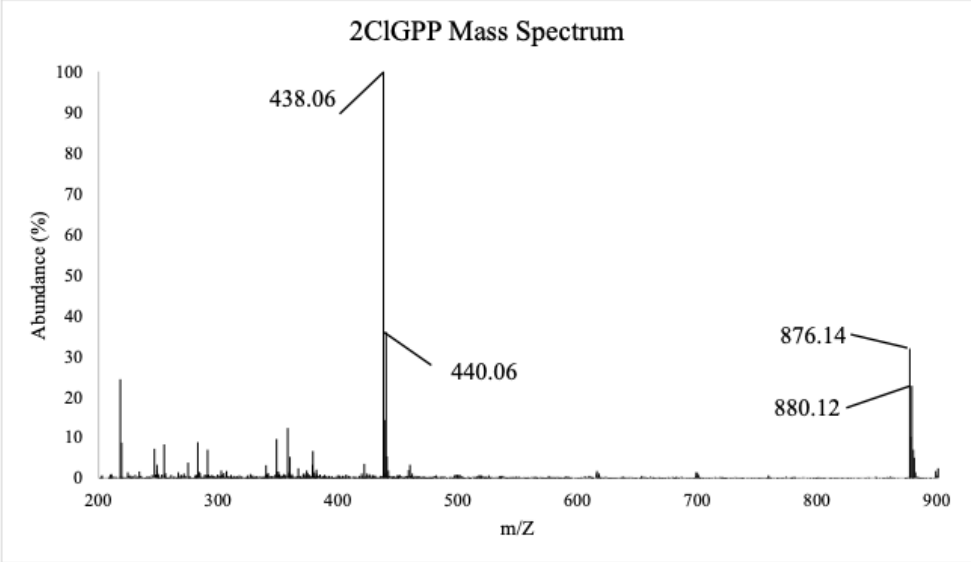

***Figure 31**: Mass spectrum for 2ClGPP*

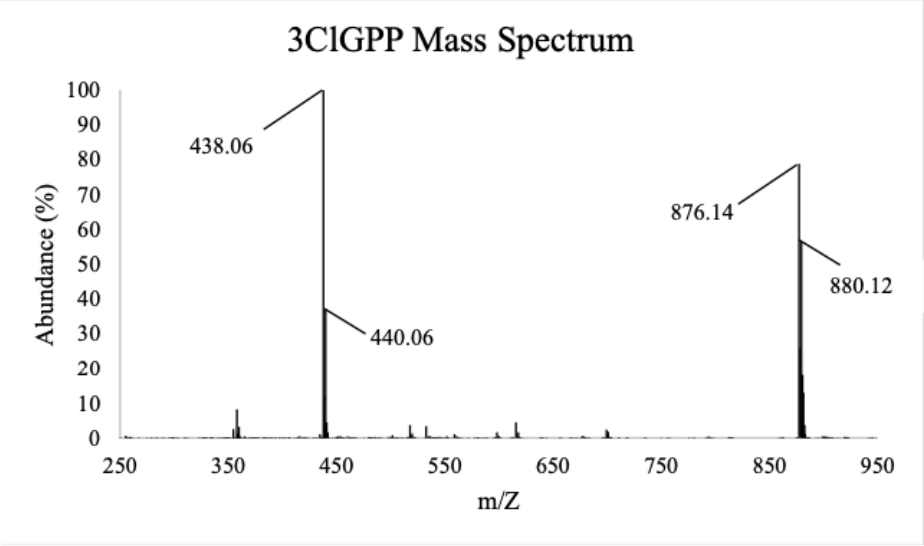

***Figure 32**: Mass spectrum for 3ClGPP*

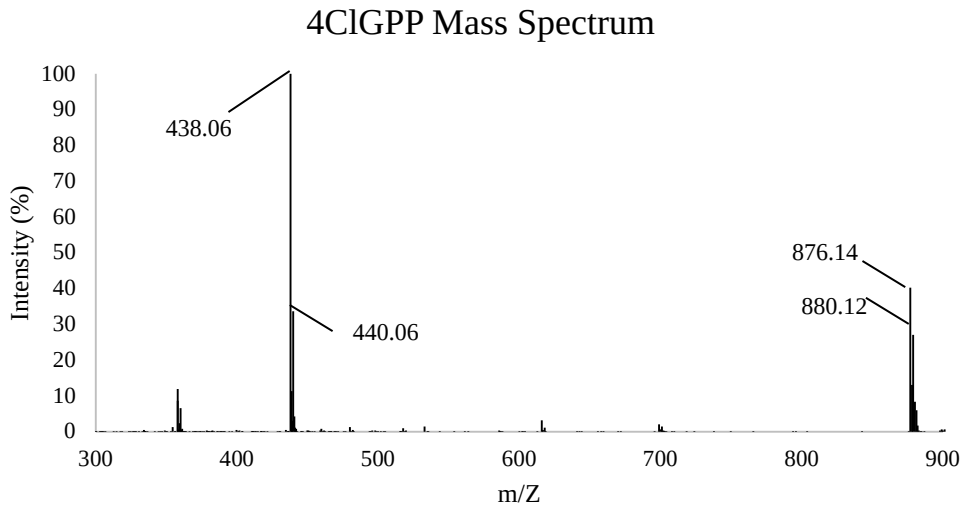

***Figure 33**: Mass Spectrum for 4ClGPP*

After the characterization of the geranyl diphosphate via mass spectrometry, UppS *S.aureus* was expressed, and purified. Protein analysis was performed via SDS-PAGE gel and a western blot (**Error! Reference source not found.**). The final concentrations were calculated spectrophotometrically with an extinction coefficient of UppS *S. a* = 36,900 M^{-1} cm^{-1} .[2] The band for UppS *S.a* can be seen at approximately 30 kDa in both SDS-PAGE gel and western blot.

The concentration of 4BrGPP was calculated to be 37.1 mM by using the extinction coefficient of the geranyl alcohol. Desired enzymatic reaction conditions were then calculated and adapted from Dodbele et. al (**Table 5**).[11] The tagged GPP, and IPP were incubated with UppS *S. aureus* along with Bicine, Potassium chloride, Magnesium chloride and the surfactant, OTG at 37 ℃. After incubation, the reaction was then tested by LCMS to see how many isoprene units, if any, were added. A gradient method of solvent A: 0.1% ammonium hydroxide, and solvent B: n-propanol 0 min: 5% B, 22.50 min: 95% B with a flow rate of 1 mL/min was used.

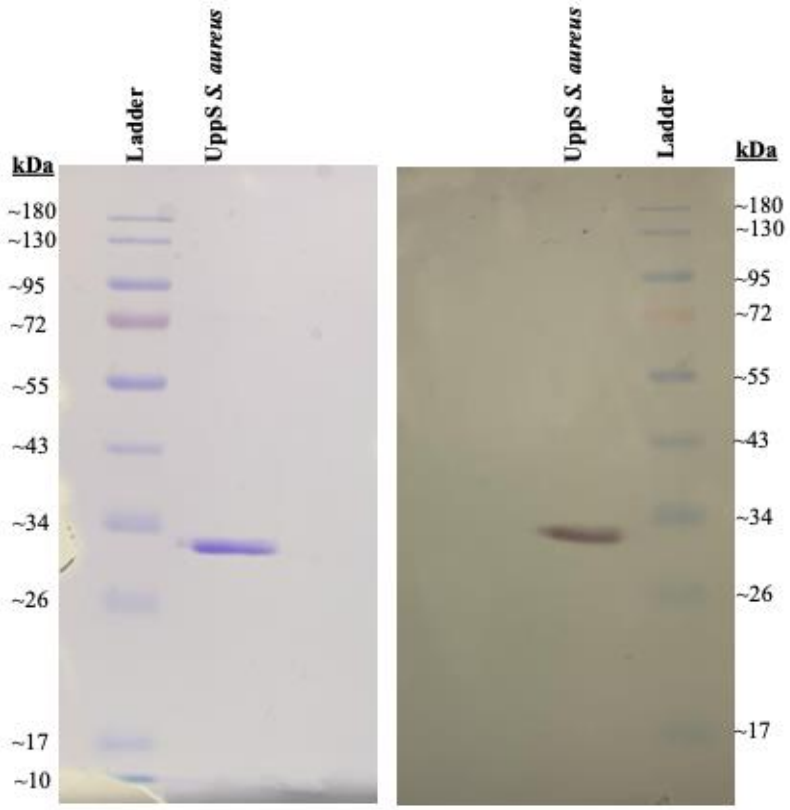

***Figure 34**: SDS-PAGE gel and Western Blot for UppS S. aureus*

***Table 5**: UppS S. aureus enzymatic reaction conditions*

Reaction Conditions	**Stock**	**Volume (μL)**
50 mM Bicine pH8	1M	25
5 mM KCl	100 mM	25
0.5 mM MgCl2	10 mM	25
2.4% OTG	10%	120
25 μM UppS *S.a*	450 μM	28
15 mM IPP	1M	7.5
2.5 mM 4BrGPP	37.1mM	20

This enzymatic reaction with conditions found in **Table 5**, resulted in the formation of 4Br(1Z)BPP and 4Br(2Z)BPP (**Figure 35**,**Figure 36**) respectively.

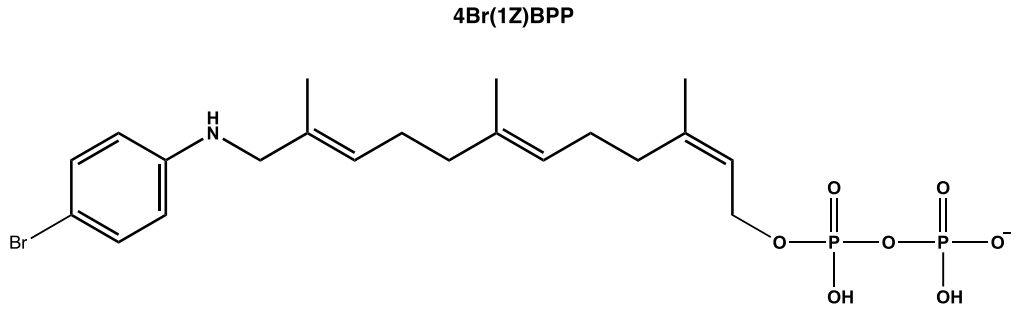

Figure 35*: Structure of 4-bromo-1Z-bactoprenyl diphosphate (4Br(1Z)BPP)*

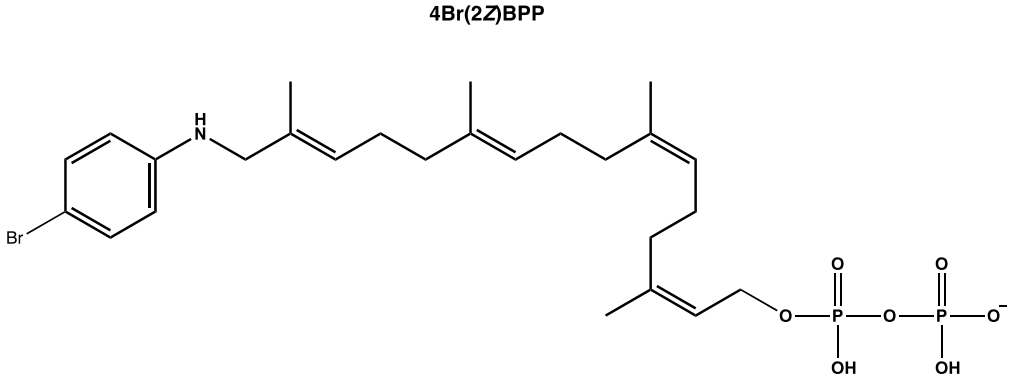

Figure 36*: Structure of 4-bromo-2Z-bactoprenyl diphosphate (4Br(2Z)BPP)*

The combined MS analysis of the BPPs scanned for zero to eight isoprene additions. The corresponding mass to charge ratios for both the chlorinated BPPs and the brominated BPPs were calculated, and analyzed using the selective ion mode (**Table 6**).

***Table 6**: Mass to charge ratios of both chlorinated and brominated bactoprenyl diphosphates for 0-8Z isoprene additions*

Isoprene Additions	**Chlorinated Bactoprenyl Diphosphates (*m/z*)**	**Brominated Bactoprenyl Diphosphates (*m/z*)**
0Z	438.06, 440.06	482.01, 484.01
1Z	506.13, 508.12	550.08, 552.07
2Z	574.19, 576.19	618.04, 620.04
3Z	646.28, 647.29	690.23, 692.23
4Z	711.32, 712.33	755.27, 757.27
5Z	779.38, 780.39	823.33, 825.33
6Z	847.45, 848.45	891.40, 893.39
7Z	914.50, 915.51	958.45, 960.45
8Z	982.56, 984.56	1026.51, 1028.51

The full spectrum of 4BrBPP showed two large peaks with retention times of about 4.5 min and 5.8 min (**Figure 37**). It was determined that the first peak at 4.5 min was the brominated BPP with 1Z isoprene addition, and the second peak at 5.8 min was the brominated BPP with 2Z isoprene additions (**Figure 37**). The mass spectrum for 4Br(1Z)BPP is shown in **Figure 38**, and clearly displayed the expected 1Z *m/z* peaks of practically equal abundance at 550.08 and 552.01 *m/z*. The mass spectra for the second signal at 5.8 min was determined to be the brominated BPP with 2 isoprene additions (**Figure 37**). This is clearly shown in **Figure 39** with practically equally abundant peaks at 618.14 and 620.14 *m/z*.

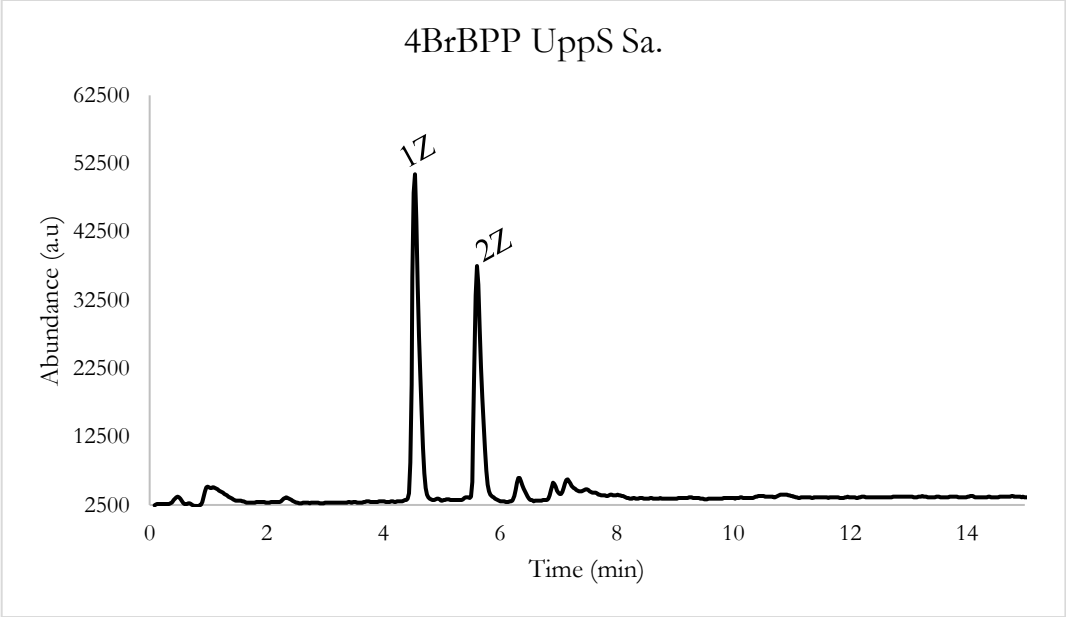

***Figure 37**: 4BrBPP from UppS S. aureus showing the first and second isoprene additions at 4.5 min and 5.8 min respectively*

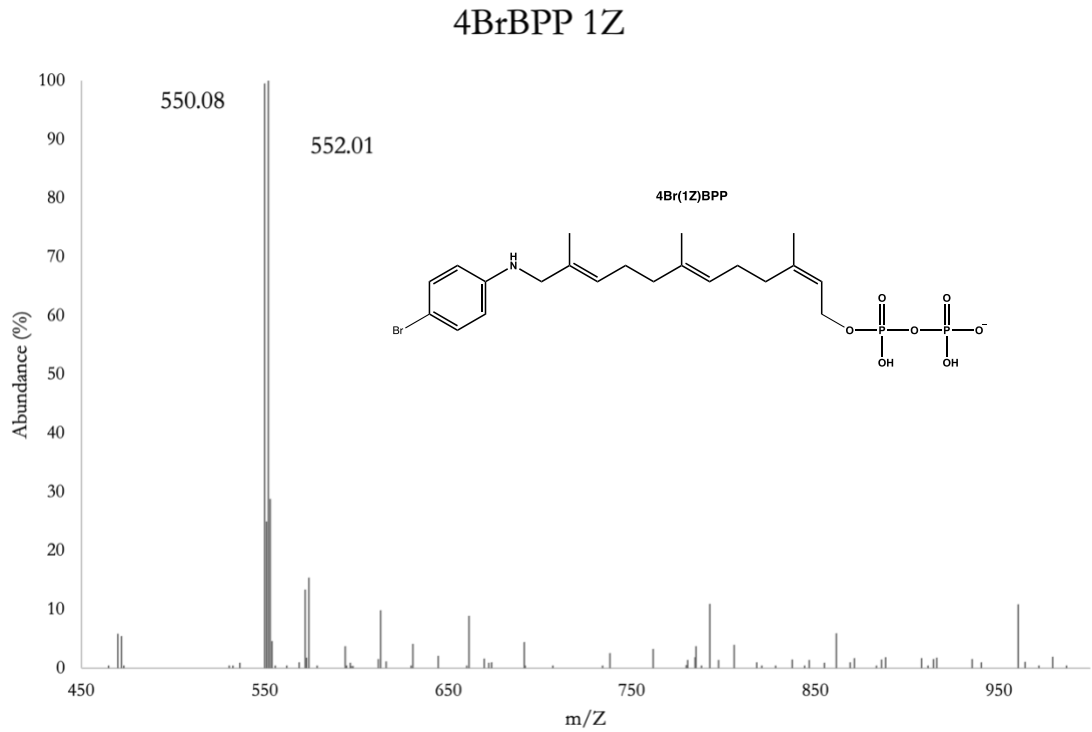

***Figure 38**: 4BrBPP 1Z mass spectrum*

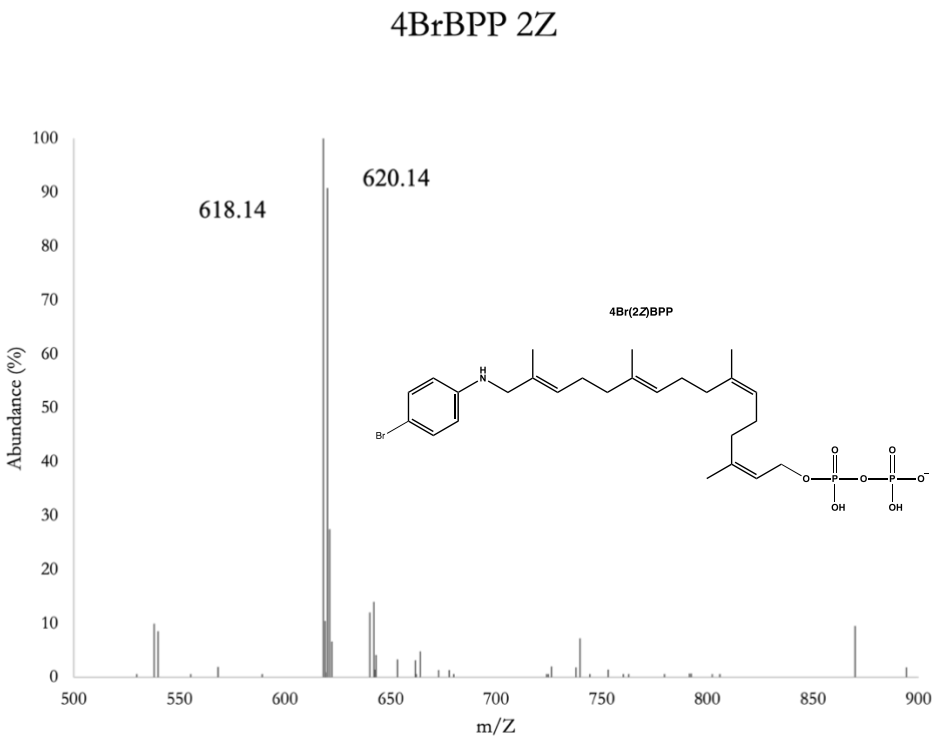

***Figure 39**: 4BrBPP 2Z mass spectrum*

The enzymatic reactions for the other chlorinated and brominated GPPs were not completed due to time constraints. The expected mass to charge ratios for the remainder of these two halogen sets of interest are found in **Table 6**. Once synthesized, it is expected that the chlorinated (438.06 *m/z*), and fluorinated analogues (422.09 *m/z*) would produce full length BPPs due to results from previous experiments with the analogue 2CNGPP, which has a similar mass to charge ratio of 429.10 *m/z*. Between the ortho, meta, and para positions for the chlorinated and fluorinated GPPs, it is hypothesized that the ortho position would be most ideal, as it is most similar to the 2CNGPP analogue. Electronegativity (EN) differences should also be taken into consideration as the 2CN tag has an EN=0.49, and the chlorine tag, with an EN difference from 2CN of 0.12, has an EN=0.61.

CHAPTER 4: CONCLUSIONS AND FUTURE WORK

4.1: Conclusions

Further understanding of the UppS active site structure and the chemical interactions of its substrates could lead to the development of inhibitors that could be targets for antimicrobial agents, and other new therapeutics. Often, the investigation of the active site of proteins employs site directed mutagenesis to alter specific amino acids associated with protein function.[5,6] However, altering amino acid structures with natural amino acids can be limiting, and close examination of structure/activity relationships can be met with difficulty due to the limited chemical space that can be explored. This thesis investigated the specificity and selectivity of the UppS enzyme through the modification of the natural substrate farnesyl diphosphate (FPP) with brominated aromatics to test the selectivity of the enzyme based on size, electronegativity, and shape.

4.1.1: Synthesis of the Alternative Substrate

Due to the past research done by the Troutman laboratory, I was able to adapt the synthesis procedure used from our previously published papers.[2,11] The original synthesis tag-appending step utilized $TiCl_4$ and pyridine to accelerate the reaction, however, this was found to be unsuccessful when applied in this study. This was attributed to the extreme water sensitivity of $TiCl_4$. To overcome this, a method change was deemed necessary and was successful in producing the desired product.

The necessity of the in-house synthesis of TTNBAPP for diphosphorylation was also problematic. During crystallization of the TTNABPP, the method stated to allow crystallization overnight at -20 °C, though it was discovered that crystallization at a higher temperature of 4 ℃ more successful.

4.1.2: Purification and Characterization of the Alternative Substrate

The purification of the alternative substrate and its' intermediates was a lengthy process due the required purification after each synthesis step. Flash chromatography was employed for steps leading up to diphosphorylation. Since obtaining an accurate weight of the geranyl diphosphate would be difficult due to the scale of the diphosphorylation reaction. To overcome this, the molar absorptivity's of the alcohols were calculated in order to determine the concentrations of the diphosphates based on the presence of aromatics.

Once the TTNBAPP was added during diphosphorylation, and the reaction was completed, it was checked by TLC. The brominated intermediate spot was expected to decrease greatly in size, while the diphosphate spot was to appear around the baseline of the plate. However, the brominated intermediate signal often did not drastically decrease even with the new appearance of the diphosphorylated product at the baseline. This led to further examination via mass spectrometry to verify the success of the reaction. It was determined that although the brominated intermediate remained on the TLC plate for the final product, the reaction still produced geranyl diphosphate.

The diphosphorylated product then required ion exchange prior to HPLC purification and enzymatic reaction, to exchange the bulky cation group from TTNBAPP to NH_4^+, which in turn allowed for clearer resolution of the X-GPP on the HPLC chromatogram.

4.1.3: Enzymatic Reaction and Analysis

UppS from *staphylococcus aureus* was expressed and used for enzymatic reaction with 4BrGPP. Incubation of UppS *S.a* with IPP and 4BrGPP produced 4BrBPP with 1 and

2 isoprene additions (**Figure 37**). This was confirmed through mass spectrometry by the presence of 2 almost equally abundant signals at 550.08 *m/z* and 552.01 m/Z for 4Br(1Z)BPP, and 618.14 *m/z* and 620.14 *m/z* for 4Br(2Z)BPP (**Figures 38,Figure 39**) respectively. The presence of 4BrBPP 1Z and 4BrBPP 2Z, proved that 4BrGPP did act as an alternative substrate for UppS *S.a.*

4.2: Future Work in UppS Alternative Substrate Synthesis and Analysis

Continuing work of this research should include the synthesis of the rest of the halogen set including fluorinated geranyl diphosphates: 2FGPP, 3FGPP, and 4FGPP, and iodinated geranyl diphosphates: 2IGPP, 3IGPP, and 4IGPP, to allow for a more complete overview on potential enzymatic activity trends. The completed set of tagged-GPPs should be characterized by mass spectrometry and by ^{1}H, ^{13}C, and ^{31}P NMR. Once characterized, the X-GPPs should be incubated with UppS *S.a*, and the enzymatic results analyzed via LCMS to determine isoprenoid length.

4.3: Future Work in UppS reactions and Analysis

Another area of interest with this work would be to do enzymatic reactions with UppS from various species. Potential species could include *Vibrio vulnificus*, *Bacteroides fragilis*, *Campylobacter jejuni*, *Helicobacter pylori,* and *Escherichia coli*. These results would give information on the potential differences between species' active sites, and therefore, broadening the range of potential therapeutic research. Altering the enzymatic reaction conditions to examine chain elongation and enzyme activity would also be of great value. Conditions to alter could include the surfactant, incubation time, and incubation temperature.

Kinetics assays on these reactions would also be of value as they would provide insight into the enzyme's catalytic mechanism, and factors that impact its activity, including mechanism of inhibition.[11] Depending on the outcome of these enzymatic assays, the next set of tags could be narrowed down even further for more information on the active site of this important enzyme.

REFERNCES

(1) Ajit Varki. Biological Roles of Glycans. *Journal of Glycobiology* **2016**, *27* (1), 3–49.

(2) Reid, A. J.; Scarbrough, B. A.; Williams, T. C.; Gates, C. E.; Eade, C. R.; Troutman, J. M. General Utilization of Fluorescent Polyisoprenoids with Sugar Selective Phosphoglycosyltransferases. *Biochemistry* **2020**, *59* (4), 615–626. https://doi.org/10.1021/acs.biochem.9b01026.

(3) Raetz, C. R. H. BIOCHEMISTRY OF ENDOTOXINS. 44.

(4) Kuo, C.-J.; Guo, R.-T.; Lu, I.-L.; Liu, H.-G.; Wu, S.-Y.; Ko, T.-P.; Wang, A. H.-J.; Liang, P.-H. Structure-Based Inhibitors Exhibit Differential Activities against *Helicobacter Pylori* and *Escherichia Coli* Undecaprenyl Pyrophosphate Synthases. *Journal of Biomedicine and Biotechnology* **2008**, *2008*, 1–6. https://doi.org/10.1155/2008/841312.

(5) Kellogg, B. A.; Poulter, C. D. Chain Elongation in the Isoprenoid Biosynthetic Pathway. *Current Opinion in Chemical Biology* **1997**, *1* (4), 570–578. https://doi.org/10.1016/S1367-5931(97)80054-3.

(6) Liang, P.-H.; Ko, T.-P.; Wang, A. H.-J. Structure, Mechanism and Function of Prenyltransferases: Structure, Mechanism and Function of Prenyltransferases. *European Journal of Biochemistry* **2002**, *269* (14), 3339–3354. https://doi.org/10.1046/j.1432-1033.2002.03014.x.

(7) Valastyan, J. S.; Lindquist, S. Mechanisms of Protein-Folding Diseases at a Glance. *Disease Models & Mechanisms* **2014**, *7* (1), 9–14. https://doi.org/10.1242/dmm.013474.

(8) Peracchi, A. Enzyme Catalysis: Removing Chemically 'Essential' Residues by Site-Directed Mutagenesis. *Trends in Biochemical Sciences* **2001**, *26* (8), 497–503. https://doi.org/10.1016/S0968-0004(01)01911-9.

(9) Richard T. Johnson. Prion Diseases. *Lancet Neurol* **2005**, *4* (42), 635–641.

(10) Muhammad Imran; Saqib Mahmood. An Overview of Animal Prion Diseases. *Virology Journal* **2011**, *8*, 493–501.

(11) Dodbele, S.; Martinez, C. D.; Troutman, J. M. Species Differences in Alternative Substrate Utilization by the Antibacterial Target Undecaprenyl Pyrophosphate Synthase. *Biochemistry* **2014**, *53* (30), 5042–5050. https://doi.org/10.1021/bi500545g.

(12) Scholte, A. Synthesis and Biological Activity of Isopentenyl Diphosphate Analogues. *Bioorganic & Medicinal Chemistry* **2004**, *12* (4), 763–770. https://doi.org/10.1016/j.bmc.2003.11.033.

(13) Chang, S.-Y.; Ko, T.-P.; Liang, P.-H.; Wang, A. H.-J. Catalytic Mechanism Revealed by the Crystal Structure of Undecaprenyl Pyrophosphate Synthase in Complex with Sulfate, Magnesium, and Triton. *Journal of Biological Chemistry* **2003**, *278* (31), 29298–29307. https://doi.org/10.1074/jbc.M302687200.

(14) Ko TP; Chen YK; Robinson H; Tsai PC; Gao YG; Chen AP; Wang AH; Liang PH. Mechanism of Product Chain Length Determination and the Role of a Flexible Loop in Escherichia Coli Undecaprenyl-Pyrophosphate Synthase Catalysis. *Journal of Biological Chemistry* **2001**, *276* (50), 47474–47482. https://doi.org/10.1074/jbc.m106747200.

(15) Chen, Y.-H.; Chen, A. P.-C.; Chen, C.-T.; Wang, A. H.-J.; Liang, P.-H. Probing the Conformational Change of Escherichia ColiUndecaprenyl Pyrophosphate Synthase during Catalysis Using an Inhibitor and Tryptophan Mutants. *Journal of Biological Chemistry* **2002**, *277* (9), 7369–7376. https://doi.org/10.1074/jbc.M110014200.

(16) Guo, R.-T.; Ko, T.-P.; Chen, A. P.-C.; Kuo, C.-J.; Wang, A. H.-J.; Liang, P.-H. Crystal Structures of Undecaprenyl Pyrophosphate Synthase in Complex with Magnesium, Isopentenyl Pyrophosphate, and Farnesyl Thiopyrophosphate. *Journal of Biological Chemistry* **2005**, *280* (21), 20762–20774. https://doi.org/10.1074/jbc.M502121200.

(17) Sing-Yang Chang; Yi-Kai Chen; Andrew H.-J. Wang; Po-Huang Liang. Identification of the Active Conformation and the Importance of Length of the Flexible Loop 72-83 in Regulating the Conformational Change of Undecaprenyl Pyrophosphate Synthase. *Journal of Biochemistry* **2003**, *42* (49), 14452–14459.

(18) Chen, A. P.-C.; Chang, S.-Y.; Lin, Y.-C.; Sun, Y.-S.; Chen, C.-T.; Wang, A. H.-J.; Liang, P.-H. Substrate and Product Specificities of *Cis* -Type Undecaprenyl Pyrophosphate Synthase. *Biochemical Journal* **2005**, *386* (1), 169–176. https://doi.org/10.1042/BJ20040785.

(19) Pan, J.-J.; Chiou, S.-T.; Liang, P.-H. Product Distribution and Pre-Steady-State Kinetic Analysis of *Escherichia Coli* Undecaprenyl Pyrophosphate Synthase Reaction. *Biochemistry* **2000**, *39* (35), 10936–10942. https://doi.org/10.1021/bi000992l.

(20) Teng, K.-H.; Liang, P.-H. Structures, Mechanisms and Inhibitors of Undecaprenyl Diphosphate Synthase: A Cis-Prenyltransferase for Bacterial Peptidoglycan Biosynthesis. *Bioorganic Chemistry* **2012**, *43*, 51–57. https://doi.org/10.1016/j.bioorg.2011.09.004.

(21) Zhu, W.; Zhang, Y.; Sinko, W.; Hensler, M. E.; Olson, J.; Molohon, K. J.; Lindert, S.; Cao, R.; Li, K.; Wang, K.; Wang, Y.; Liu, Y.-L.; Sankovsky, A.; de Oliveira, C. A. F.; Mitchell, D. A.; Nizet, V.; McCammon, J. A.; Oldfield, E. Antibacterial Drug Leads Targeting Isoprenoid Biosynthesis. *Proc. Natl. Acad. Sci. U.S.A.* **2013**, *110* (1), 123–128. https://doi.org/10.1073/pnas.1219899110.

(22) Lee, L. V.; Granda, B.; Dean, K.; Tao, J.; Liu, E.; Zhang, R.; Peukert, S.; Wattanasin, S.; Xie, X.; Ryder, N. S.; Tommasi, R.; Deng, G. Biophysical Investigation of the Mode of Inhibition of Tetramic Acids, the Allosteric Inhibitors of Undecaprenyl Pyrophosphate Synthase. *Biochemistry* **2010**, *49* (25), 5366–5376. https://doi.org/10.1021/bi100523c.

(23) Guo, R.-T.; Cao, R.; Liang, P.-H.; Ko, T.-P.; Chang, T.-H.; Hudock, M. P.; Jeng, W.-Y.; Chen, C. K.-M.; Zhang, Y.; Song, Y.; Kuo, C.-J.; Yin, F.; Oldfield, E.; Wang, A. H.-J. Bisphosphonates Target Multiple Sites in Both *Cis* - and *Trans* - Prenyltransferases. *Proc. Natl. Acad. Sci. U.S.A.* **2007**, *104* (24), 10022–10027. https://doi.org/10.1073/pnas.0702254104.

(24) Sinko, W.; Wang, Y.; Zhu, W.; Zhang, Y.; Feixas, F.; Cox, C. L.; Mitchell, D. A.; Oldfield, E.; McCammon, J. A. Undecaprenyl Diphosphate Synthase Inhibitors: Antibacterial Drug Leads. *J. Med. Chem.* **2014**, *57* (13), 5693–5701. https://doi.org/10.1021/jm5004649.

(25) Yunlei Guo; Guanhui Song; Meiling Sun; Juan Wang; Yi Wang. Prevalence and Therapies of Antibiotic-Resistance in Staphylococcus Aureus. *Frontiers in Cellular and Infection Microbiology* **2020**, *10* (107), 1–11.

(26) Chen, A. P.-C.; Chen, Y.-H.; Liu, H.-P.; Li, Y.-C.; Chen, C.-T.; Liang, P.-H. Synthesis and Application of A Fluorescent Substrate Analogue to Study Ligand Interactions for Undecaprenyl Pyrophosphate Synthase. *J. Am. Chem. Soc.* **2002**, *124* (51), 15217–15224. https://doi.org/10.1021/ja020937v.

(27) Teng, K.-H.; Chen, A. P.-C.; Kuo, C.-J.; Li, Y.-C.; Liu, H.-G.; Chen, C.-T.; Liang, P.-H. Fluorescent Substrate Analog for Monitoring Chain Elongation by Undecaprenyl Pyrophosphate Synthase in Real Time. *Analytical Biochemistry* **2011**, *417* (1), 136–141. https://doi.org/10.1016/j.ab.2011.05.043.

(28) Amanda J. Reid; Jerry Troutman; Joseph M. Hazel; Vinita Lukose; Katelyn M. Erickson. Preparation and Immobilization of a Bacterial Oligosaccharide for Glycan Binding Partner Recognition.

(29) Yao-Wen Wu; Kirill Alexandrov; Luc Brunsveld. Synthesis of a Fluorescent Analogue of Geranylgeranyl Pyrophosphate and Its Use in a High-Throughput Fluorometric Assay for Rab Geranylgeranyltransferase. *Nature Protocols* **2007**, 2704–2711.

(30) Amanda J. Reid; Beth Scarbrough; Jerry Troutman; Claire E. Gates; Tiffany Williams; Colleen Eade. Preparation and Immobilization of a Bacterial Oligosaccharide for Glycan Binding Partner Recognition.

(31) G. Popjak; J.W. Cornforth; Rita H. Cornforth; R. Ryhage; DeWitt S. Goodman. Studies on the Biosynthesis of Cholesterol: *The Journal of Biological Chemistry* **1962**, *237* (1), 56–61.

(32) Hooff, G. P.; Peters, I.; Wood, W. G.; Müller, W. E.; Eckert, G. P. Modulation of Cholesterol, Farnesylpyrophosphate, and Geranylgeranylpyrophosphate in Neuroblastoma SH-SY5Y-APP695 Cells: Impact on Amyloid Beta-Protein Production. *Mol Neurobiol* **2010**, *41* (2–3), 341–350. https://doi.org/10.1007/s12035-010-8117-5.

(33) Palsuledesai, C. C.; Distefano, M. D. Protein Prenylation: Enzymes, Therapeutics, and Biotechnology Applications. *ACS Chem. Biol.* **2015**, *10* (1), 51–62. https://doi.org/10.1021/cb500791f.

(34) Owen, D. J.; Alexandrov, K.; Rostkova, E.; Scheidig, A. J.; Goody, R. S.; Waldmann, H. Chemo-Enzymatic Synthesis of Fluorescent Rab 7 Proteins: Tools to Study Vesicular Trafficking in Cells. *Angew. Chem. Int. Ed.* **1999**, *38* (4), 509–512. https://doi.org/10.1002/(SICI)1521-3773(19990215)38:4<509::AID-ANIE509>3.0.CO;2-3.

(35) Samuel L. Scinto; Joseph M. Fox. Bioorthogonal Chemsitry, 2021. https://www.ncbi.nlm.nih.gov/pmc/articles/PMC8469592/.

(36) Wang, Y.-C.; Distefano, M. D. Synthetic Isoprenoid Analogues for the Study of Prenylated Proteins: Fluorescent Imaging and Proteomic Applications. *Bioorganic Chemistry* **2016**, *64*, 59–65. https://doi.org/10.1016/j.bioorg.2015.12.003.

(37) Wang, Q.; Chan, T. R.; Hilgraf, R.; Fokin, V. V.; Sharpless, K. B.; Finn, M. G. Bioconjugation by Copper(I)-Catalyzed Azide-Alkyne [3 + 2] Cycloaddition. *J. Am. Chem. Soc.* **2003**, *125* (11), 3192–3193. https://doi.org/10.1021/ja021381e.

(38) Saxon, E.; Bertozzi, C. R. Cell Surface Engineering by a Modified Staudinger Reaction. *Science* **2000**, *287* (5460), 2007–2010. https://doi.org/10.1126/science.287.5460.2007.

(39) Troutman, J. M.; Roberts, M. J.; Andres, D. A.; Spielmann, H. P. Tools To Analyze Protein Farnesylation in Cells. *Bioconjugate Chem.* **2005**, *16* (5), 1209–1217. https://doi.org/10.1021/bc050068+.

(40) Gurung, A. B.; Researcher; Bhattacharjee, A.; Assistant Professor, Computational Biology Laboratory, Department of Biotechnology & Bioinformatics, North Eastern Hill University, Shillong, India. Significance of Ras Signaling in Cancer and Strategies for Its Control. *Oncology & Hematology Review (US)* **2015**, *11* (02), 147. https://doi.org/10.17925/OHR.2015.11.02.147.

(41) Hahne, K.; Vervacke, J. S.; Shrestha, L.; Donelson, J. L.; Gibbs, R. A.; Distefano, M. D.; Hrycyna, C. A. Evaluation of Substrate and Inhibitor Binding to Yeast and Human Isoprenylcysteine Carboxyl Methyltransferases (Icmts) Using Biotinylated Benzophenone-Containing Photoaffinity Probes. *Biochemical and Biophysical Research Communications* **2012**, *423* (1), 98–103. https://doi.org/10.1016/j.bbrc.2012.05.089.

(42) Anderson, J. L.; Henriksen, B. S.; Gibbs, R. A.; Hrycyna, C. A. The Isoprenoid Substrate Specificity of Isoprenylcysteine Carboxylmethyltransferase. *Journal of Biological Chemistry* **2005**, *280* (33), 29454–29461. https://doi.org/10.1074/jbc.M504982200.

(43) Turek, T. C.; Gaon, I.; Distefano, M. D. Analogs of Farnesyl Pyrophosphate Incorporating Internal Benzoylbenzoate Esters: Synthesis, Inhibition Kinetics and Photoinactivation of Yeast Protein Farnesyltransferase. *Tetrahedron Letters* **1996**, *37* (28), 4845–4848. https://doi.org/10.1016/0040-4039(96)00972-0.

(44) Edelstein, R. L.; Distefano, M. D. Photoaffinity Labeling of Yeast Farnesyl Protein Transferase and Enzymatic Synthesis of a Ras Protein Incorporating a Photoactive Isoprenoid. *Biochemical and Biophysical Research Communications* **1997**, *235* (2), 377–382. https://doi.org/10.1006/bbrc.1997.6792.

(45) Chehade, K. A. H.; Kiegiel, K.; Isaacs, R. J.; Pickett, J. S.; Bowers, K. E.; Fierke, C. A.; Andres, D. A.; Spielmann, H. P. Photoaffinity Analogues of Farnesyl Pyrophosphate Transferable by Protein Farnesyl Transferase. *J. Am. Chem. Soc.* **2002**, *124* (28), 8206–8219. https://doi.org/10.1021/ja0124717.

(46) Igor Gaon; Tammy C. Turek; Mark D. Distefano. Farnesyl and Geranylgeranyl Pyrophosphate Analogues Incorporating Benzoylbenzyl Ethers: Synthesis and Inhibition of Yeast Protein Farnesyltransferase. *Tetrahedron Letters* **1996**, *37* (49), 8833–8836.

(47) Kim; Kleckley, T. S.; Wiemer, A. J.; Holstein, S. A.; Hohl, R. J.; Wiemer, D. F. Synthesis and Activity of Fluorescent Isoprenoid Pyrophosphate Analogues. *J. Org. Chem.* **2004**, *69* (24), 8186–8193. https://doi.org/10.1021/jo049101w.

(48) Davisson, V. J.; Woodside, A. B.; Neal, T. R.; Stremler, K. E.; Muehlbacher, M.; Poulter, C. D. Phosphorylation of Isoprenoid Alcohols. *J. Org. Chem.* **1986**, *51* (25), 4768–4779. https://doi.org/10.1021/jo00375a005.

(49) Jungjoo Nam; Hyuksu Kwon; Inae Jang; Aeran Jeon; Jingyu Moon; Sun Young Lee; Dukjin Kang; Sang Yun Han; Bongjin Moon; Han Bin Oh. Bromine Isotopic Signature Facilitates de Novo Sequencing of Peptides in Free-Radical-Initiated Petide Sequencing (FRIPS) Mass Spectrometry. *Journal of Mass Spectrometry* **2015**, *50* (2), 378–387.

(50) Throck J. Watson; David O. Sparkman. *Introduction to Mass Spectrometry*, 4th ed.; 2007.

(51) Prof. Dr. F. Cramer; W. Bohm. Synthese von Geranyl- Und Farnesyl-Pyrophosphat. *Angewandte Chemie International Edition* **1959**, *71* (24), 775.

(52) Vyas M. Dixit; F. Mark Laskovics; Wendy I. Noall; C. Dale Poulter. Tris(Tetra-n-Butylammonium) Hydrogen Pyrophosphate. A New Reagent for the Preparation of

Allylic Pyrophosphate Esters. *Journal of Organic Chemistry* **1981**, *46* (9), 1967–1969.